CFD simulation of flow fields associated with high speed jet impingement on deflectors

Robert Gordon Garcia

Thesis submitted to the Faculty of the
Virginia Polytechnic Institute and State University
In fulfillment of the requirements for the degree of

Master of Science
In
Mechanical Engineering

Dr. Walter F. O'Brien, Chair
Dr. Mark Paul
Dr. Danesh Tafti

April 6, 2007
Blacksburg, Virginia

Keywords: CFD, Underexpanded Jets, Impingement, Jet deflectors

CFD simulation of flow fields associated with high speed jet impingement on deflectors

Robert G. Garcia

Abstract

Computational Fluid Dynamics is used to analyze the formation of under-expanded jets and to investigate the three-dimensional flow field associated with the impingement of free jets onto stationary deflectors. This investigation was performed to develop a verified modeling ability for such problems. Predictions were compared with the experimental results obtained by Donaldson and Snedeker [1]. Computational models for free and impinging jets were created according to the data provided in Ref. 1. Numerical results for each of the experiments performed in this benchmark report are presented.

Three different turbulent free jets produced by a simple convergent nozzle were analyzed. These include a subsonic jet with $p_1/p_\infty=1$ and $M_1=0.57$, a moderately under-expanded jet with $p_1/p_\infty=1.42$ and $M_1=1$, and a highly under-expanded jet with $p_1/p_\infty=3.57$ and $M_1=1$. The reflecting shocks associated with the moderately under-expanded jet as well as the shock disk associated with the highly under-expanded jet were fully resolved. Velocity profile data predicted at locations downstream of the nozzle exit agreed very well with the experimental results.

The impingement of a moderately under-expanded jet with $p_1/p_\infty=1.42$ and $M_1=1$ was also investigated. The interaction of the high speed jet with circular flat plates at angles of 60º and 45º relative to the center axis of the jet are presented. Wall jet velocity

profiles on the surface of the flat plate are fully resolved and compare well with experimental results. The CFD solver controls and method used to obtain these results are summarized and justified.

Acknowledgments

I would like to thank Dr. O'Brien for providing me with the opportunity to work on this research project and the others I have contributed to during my graduate education. Through his guidance and expertise in aircraft related flows, I have gained invaluable skills and knowledge that I will surely use throughout my career. I would also like to thank Dr. Paul and Dr. Tafti for supporting my research and academic goals. I would like to thank my parents Robert and Connie Garcia for their love and support throughout my seven years here at Virginia Tech. Finally, I would like to thank my partner Sarah for always reminding that a balance of work and family is necessary for a happy life.

Table of Contents

CFD simulation of flow fields associated with high speed jet impingement on deflectors

List of Figures

List of Tables

Nomenclature

A_{cell} Cell Area

A_0 Model Constant

A_s Model Constant, $A_s = \sqrt{6}\cos\phi$

C_1 Model Constant, $C_1 = \max\left[0.43, \frac{\eta}{\eta+5}\right]$

C_2 Model Constant

$C_{1\varepsilon}$ Model Constant

$C_{3\varepsilon}$ Model Constant

C_μ Coefficient of Eddy Viscosity, $C_\mu = \frac{1}{A_0 + A_S \frac{kU^*}{\varepsilon}}$

e_{i1} Error Indicator

G_k Generation of Turbulence Kinetic Energy due to the Mean Velocity Gradients

k Turbulence Kinetic Energy

r Gradient Volume Weight

$\vec{r}$ Displacement Vector from the Upstream Cell Centroid to the Face Centroid

S_k Magnitude of the strain rate tensor

S_ε User-Defined Source Term of Turbulence Dissipation

S Model Constant, $S = \sqrt{2S_{ij}S_{ij}}$, $\tilde{S} = \sqrt{S_{ij}S_{ij}}$

S_{ij} Acceleration Tensor, $S_{ij} = \frac{1}{2}\left(\frac{\partial u_j}{\partial x_i} + \frac{\partial u_i}{\partial x_j}\right)$

t Time

u Velocity Component

U^* Coefficient of Velocity, $U^* = \sqrt{S_{ij}S_{ij} + \tilde{\Omega}_{ij}\tilde{\Omega}_{ij}}$

W Coefficient of Relative Velocity, $W = \frac{S_{ij}S_{jk}S_{ki}}{S^3}$

x Cartesian Coordinate

Y_M Contribution of the Fluctuating Dilatation in Compressible Turbulence due to the Overall Dissipation Rate

η Model Constant, $\eta = S\frac{k}{\varepsilon}$

ε Dissipation Rate

ε_{ijk} Alternating Unit Tensor

μ_t Turbulent Viscosity, $\mu_t = \rho C_\mu \frac{k^2}{\varepsilon}$

ρ Density

μ Dynamic Viscosity

σ_k Turbulent Prandtl Number for k

σ_ε Turbulent Prandtl Number for ε

ν Kinematic Viscosity

ϕ Model Constant, $\phi = \frac{1}{3}\cos^{-1}\left(\sqrt{6}W\right)$

ϕ_c Computational Result

ϕ_e Experimental Result

ϕ_f Face Value of a Given Parameter

ϕ_n Nodal Value of a Given Parameter

ϕ Given Parameter

$\bar{\phi}$ Time Averaged Parameter

ϕ' Fluctuating component of a specified Parameter

$\phi_{f,SOU}$ Cell Centered Value for the Second Order Upwind Discretization Scheme

ϖ_k Angular Velocity

Ω_{ij} Rate-of-Rotation Tensor, $\Omega_{ij} = \overline{\Omega_{ij}} - \varepsilon_{ijk}\varpi_k$

$\tilde{\Omega}_{ij}$ Mass Averaged Rate-of-Rotation Tensor, $\tilde{\Omega}_{ij} = \Omega_{ij} - 2\varepsilon_{ijk}\varpi_k$

ξ Percent Error

i,j,k Index Notation

∇ Vector Differential Operator

∇f Euclidian Norm of the Gradient in the Desired Field Variable, f

1 Introduction

1.1 Research Objectives

The primary goal of the current research was to provide a computational model for the analysis of high speed jet impingement. This model can be used to predict the entrainment of quiescent air through angled channels due to the deflection of high velocity jets. Use of the commercial software package FLUENT [2] enabled the objectives of this research to be achieved. In development of the computational model, the formation and structure of subsonic and underexpanded jets were investigated. Experimental results for free jets and free jet impingement obtained in previous investigations provided the necessary data for validation of the computational model. The ability of FLUENT to accurately model and predict the flowfield effects due to the impingement of high speed jets was quantified. Inlet boundary conditions and solution controls required to accurately model circular jets are presented.

1.2 Significance of the Current Research

The interaction of free jets and deflectors has been studied since the 1950s. Effects due to this flowfield are observed in many applications and continue to remain the focus of many research projects today. Use of CFD for the analysis of high speed jet impingement provides a complete characterization of the flowfield, enabling further insight into the flow structure. Development of the upstream flow as well as interaction with the surrounding environment can now be observed. CFD provides resolution of the flowfield that would otherwise be impossible due to the inherent unsteadiness of the flow.

Through the completion of this investigation, flow effects due to free and impinging jets are quantified.

In addition to resolving the flowfield of impinging jets, the current investigation focused on the entrainment of fluid into both free and deflected jets. An accurate prediction of entrainment ensures that turbulent regions of the jet are modeled correctly. The interaction of the high speed jet and the surrounding environment directly affects the downstream flowfield. Early investigations of high speed jets did not provide an account of this phenomenon. It is a goal of this research to provide insight into the entire flow region affected by the formation of high speed jets and the deflection of high speed jets.

1.3 Challenges of the Analysis

There are many factors that directly affected the choice to complete this investigation computationally. The complexity associated with an analysis involving the deflection of hot jet exhaust is extremely high. The resources required to complete a full-scale investigation of this flow field are huge. Experimental testing with an actual jet engine and deflector would be impractical. In addition to the expensive equipment, a skilled workforce would be required to be on hand at all times to ensure the safe operation of each component. Due to constraints on space, time, and money, the following investigation has been completed through the use of Computational Fluid Dynamics (CFD).

Similar to the challenges associated with experimental testing, the extreme temperature and speed of the jet flow under consideration also presents challenges related to the development of a CFD model. The inherent unsteadiness and turbulence

associated with the deflection of hot jet exhaust is a very complicated flow to predict. Complete validation of the computational model is required to ensure that the results are accurate. The ability to predict a circular free jet was first investigated. Experimental results for a free jet are widely available and provide the necessary validation. In addition, the impingement of an underexpanded jet was also investigated. These cases provided a method to determine the solver controls and grid resolution necessary to accurately model the flows related to high speed jet impingement.

Another challenge in the development of an accurate CFD model was the range of length scales necessary for modeling the entrainment of fluid resulting from the deflected jet. The ideal control volume necessary to accurately model all of the effects due to the impingement of jet exhaust would be enormous. An intelligent use of grid resolution was necessary to accurately model the entrainment of air within the region of the deflector while ensuring reasonable compute time for each solution. Use of a parallel system of computers also provided the vast amount of computing resources required for this investigation to take place.

1.4 CFD and the Anantham Cluster

Use of CFD to analyze complex flows has increased exponentially since the first numerical solution techniques for fluid mechanics problems were developed by Richardson in 1910. This was a point iterative scheme for solving Laplace's equation. The numerical solutions of partial differential equations were then presented by Courant, Friedrichs, and Lewy (CFL) in 1928. Then during and after WWII there began a large amount of research on the use of numerical methods for solving problems in fluid

dynamics. With the advancement of computer technology also came the advancement of iterative solvers and algorithms. Since the introduction of the first commercially available CFD code in the 1980s, codes have been developed to analyze flows related to almost every industrial application imaginable.

All computations for this investigation were performed through use of the commercial software package FLUENT [2] on the Anantham cluster maintained by the Computer Science Department of Virginia Tech. Anantham is a 100 node Linux cluster that is interconnected over Myrinet interfaces, which use MPI directly over the underlying general messaging communication platform. Each node of Anantham has an AMD Opteron 1.4 GHz CPU with 1GB of main memory and 10GB HDD. Use of this cluster has proven to be a necessary tool for the completion of this analysis. The large scales associated with the development of a jet exhaust plume in combination with the high resolution necessary to resolve the turbulent mixing requires a vast amount of computer resources, which Anantham is able to provide.

1.5 Thesis Summary

A review of the various topics related to the development of the computational model used to predict the deflection of a high speed jet are presented in Chapter 2. Experimental and numerical investigations on free jets are first introduced. A review of jet impingement studies are then reviewed in the following subsection. The results obtained from these previous investigations provide the tools necessary to develop an accurate computational model. Investigations on the formation of shear layers and the entrainment of fluid are then reviewed. The development of computational models to

accurately predict turbulence was essential to the successful completion of this investigation.

The computational model developed for this investigation is then presented in Chapter 3. A discussion on the Reynolds Averaged Navier-Stokes equations, viscous equations, computational grid, and discretization methods used for this investigation are provided.

Chapter 4 then provides a review of the computational results obtained for the analysis of underexpanded free jets and the impingement of a moderately underexpanded free jet.

Then, based on the results presented in Chapter 4, conclusions gained from this analysis are presented in Chapter 5. Recommendations for future work are also provided in this chapter.

2 Background

2.1 Previous Studies on Free jets

Jet flows have a wide range of applications in the engineering field and have been a subject of study for centuries. The use of jets as a means of propulsion can be dated back to the first century A.D., when the Greek engineer Hero of Alexandria invented the first steam engine known as the aeolipile. This invention directed trapped steam through a pair of nozzles in order to spin a sphere very rapidly. Nozzles were also used by the Chinese in the 11th century with the invention of the rocket. Then with the invention of the first turbojet engine by Frank Whittle in the 1930s, jet propulsion introduced a way of reaching speeds before unimaginable by man.

The formation of a free jet is common to applications that involve exhaust plumes from propulsion systems, vents in high pressure systems, injection of gas into liquids, and many others. Although seeming relatively simple, circular free jets involve complex phenomena such as turbulent mixing, shocks, heat transfer coupling, and other compressibility effects. To aid in understanding these phenomena many studies have been performed on a wide range of jet flows. For the present study, the formation and decay of axisymmetric underexpanded free jets issuing from a circular convergent nozzle were of considerable importance.

A significant amount of research on the structure of turbulent free jets was conducted in the 1950s. Krzywoblocki [3] provides an in-depth review of studies on the decay of subsonic jets issuing from round nozzles into a quiescent medium. Additionally, through the work of Anderson and Johns [4], Seddon and Haverty [5], and Owen and Thornhill [6], analytical and semi-empirical methods for determining jet

characteristics of subsonic jets were developed. These studies provided an understanding of the flow within the core region of a subsonic jet.

As rocket propulsion became more widely utilized, studies on the development and decay of underexpanded jets began in the early 1960s. Love et al. [7] studied the strength and location of the initial shock structure of axisymmetric free jets. Jet stability and sound generation studied by Hammitt [8] provided further insight into the flowfield associated with underexpanded sonic jets.

It was not until the 1970's that the decay and spreading rates associated with both subsonic and sonic jets were characterized. Donaldson and Snedeker [1] used pitot and static pressure probes to develop velocity profiles and spreading and decay characteristics for a subsonic jet, a moderately underexpanded sonic jet, and a highly underexpanded sonic jet. This investigation provided the first characterization of the reflecting shock structure associated underexpanded jets and quickly became an important reference for the majority of studies on free jets that followed.

2.2 CFD Investigations on Free Jets

The advancement of computer technology throughout the past 40 years has provided an immeasurable resource for the study of fluid mechanics problems. It is now possible to assign homework problems in CFD that would have been a major breakthrough or could have formed the basis of a Ph.D. dissertation in the 1950s or 1960s. Numerical investigations provide a method for fully quantifying all parameters of a flowfield that may otherwise be too costly or just impossible to obtain experimentally.

In the early 1980s, Dash et al. [9] made considerable contributions to the numerical analysis of axisymmetric exhaust plumes. These included studies on shock processes of supersonic jets, viscous and inviscid effects, and jet mixing effects. In the 1985 study of turbulent underexpanded jets, Dash et al. [10] developed a parabolized Navier-Stokes model that solved a fully coupled system of viscous/inviscid equations. They found that the coupled model accurately related the effect of turbulent mixing processes on wave structure.

In his study on the structure of turbulent sonic underexpanded free jets in 1989, Chuech et al. [11] used a modified k-ε turbulence model to predict the turbulent mixing associated with the injection of a moderately underexpanded free jet into quiescent air. The k-ε model was modified to treat compressibility effects at high convection Mach numbers. The correction incorporated the convective Mach number of the mixing layer into the definition of the turbulent viscosity. Use of this model showed successful prediction of the constant-pressure portions of underexpanded jets.

Later in the 1990s, Woodmansee and Dutton [12] successfully used a Reynolds-averaged Navier-Stokes (RANS) system of equations with a two equation k-ε turbulence model to predict the flowfield of an underexpanded sonic jet. They were able to obtain Mach number distributions upstream of the Mach disk that compared favorably with other experimental data. Solution methods developed in these numerical studies were incorporated into the present research in order to provide an accurate prediction of the jet exhaust conditions under consideration.

2.3 Previous Studies on Free Jet Impingement

Investigations on high speed jet impingement have also remained considerably important since the 1960s. This flow situation is common to many engineering applications such as V/STOL aircraft, the takeoff and landing of rockets, various heating and cooling applications, and the deflection of exhaust from launch vehicles. The earliest investigations on jet impingement were primarily focused on improving the lift of V/STOL aircraft and understanding erosion effects on the ground below. Henderson [13] was the first to measure the pressure distribution on the surface of a circular flat plate when impinged by airstreams of various Mach numbers. This was the first investigation to study the effect of different impingement angles on surface pressure distribution.

In their 1970 study of underexpanded free jets, Donaldson and Snedeker [1] also investigated the flowfield associated with free jet impingement. The goal of their research was to fully characterize the flow resulting from the impingement of an axisymmetric turbulent jet against a circular disk whose diameter is large compared to that of the jet. Measurements of the wall jet velocity profile, heat transfer at the stagnation point, and wall surface pressure distribution were obtained for a subsonic jet, moderately underexpanded jet, and highly underexpanded jet impinging on disks at angles ranging from 90° to 45° relative to the jet centerline axis. Streamline patterns obtained from grease streaks provided a method of viewing velocity or pressure gradients on the surface of the disk. Donaldson and Snedeker's study on the decay and spreading of underexpanded jets and of free jet impingement provides the necessary experimental data for validation of the computational model developed in the present investigation.

2.4 CFD Investigations on Impinging Jets

Similarly to investigations of free jets, the use of CFD for characterizing the flowfield associated with the impingement of high speed jets provides clarity and extends the capacity of traditional experimental testing. The first numerical investigations to address issues related to jet impingement were conducted in the 1980s. These included the development of turbulent models to accurately predict flows in the near wall region.

A high Reynolds number form of the k-ε viscous model developed by Lam and Bremhorst [14] was used to predict fully developed pipe flow. By incorporating functions for the turbulent viscosity and for both high and low Reynolds numbers based on previous studies, the modified k-ε model was shown to be valid throughout the fully turbulent, semi-laminar and laminar regions within the flow. Unlike previous attempts to model fully developed pipe flow, the addition of formulas and terms for computing wall functions and completing the transport equations were not required.

Boundary conditions at solid walls were investigated further by Chen and Patel [15] in their study of flow over an axisymmetric body. Previous investigations of flows in the near wall region did not address complex phenomena such as unsteadiness and separation. Chen and Patel developed a two-layer modeling approach that would be accurate in both the inner and outer flow region. The k-ε model developed by Lam and Bremhorst [14] in addition to a one equation model used by Wolfshtein [16] were used to successfully calculate unseparated and separated flows in the wake of the axisymmetric body. The development of this model enabled the analysis of many other complicated flows.

As computer technology became more advanced, it became possible to numerically investigate jet impingement. In the 1996 study conducted by Kannenberg and Boyd [17], a full 3-D model was developed to investigate flows associated with spacecraft landing surfaces. The numerical code used was based on a direct simulation model primarily used for 2-D and axisymmetric flows. Excellent agreement to experimental data for jet impingement at various angles was found.

Numerical investigations of high speed jet impingement were again revisited by Angioletti et al. [18] in order to determine CFD performance dependence on Reynolds number. Both experimental and computational approaches were used to analyze jet impingement heat transfer. The accuracy of three commercially available turbulence models was determined by comparing velocity and local Nusselt number distributions on the impinged surface. These included the k-ε Reynolds-Normalized Group (RNG), k-ω Shear Stress Transport (SST)), and Reynolds Stress Model (RSM) turbulence models. Used in combination with the standard RANS equations, the most accurate turbulence model for low Reynolds numbers was found to be the k-ω SST model, while for high Reynolds numbers the k-ε RNG model showed considerable improvement.

Previous investigations on the use of CFD for the analysis of high speed jet impingement show excellent agreement to experimental data. The computational model and governing equations used in these investigations provide an estimate of the model requirements for the present research. By incorporating these results into the governing equations presented in the following chapter, successful validation of the computational model was achieved.

2.5 Formation of Separated Shear Layers

A method of passively cooling deflectors has been proposed that involves the entrainment of quiescent air through a series of internal channels. Entrained airflow through the channels provides the necessary heat transfer from the deflector surface. The cooling airflow results from the formation of vortices along the top edge of the disc when the deflected jet leaves the surface. The formation of such vortices is common to many engineering applications and is known as a separated shear layer.

Separated shear layers and the phenomena associated with them were extensively studied in a series of experiments conducted by Brown and Roshko [19]. Their experiments served to provide an understanding of density difference effects on mean flow as well as turbulent flow structure. The plane mixing layer between gasses of different densities and velocities were closely investigated. Shadowgraphs, such as the one shown in Figure 2.1, clearly demonstrate that mixing and entrainment occurs primarily in the formation of large eddies. Relationships were developed that provide an estimate of the amount of fluid volume entrained as a function of the average frequency that the large eddies pass a given location. Additionally, it was determined that if one of the two interacting fluids is at rest, then it is this fluid that becomes entangled with and entrained into the higher velocity fluid.

Figure 2.1. A study on the formation of separated shear layers by Brown and Roshko provides a discussion on the entrainment of fluid.

Within the past 30 years, the successful prediction of turbulent mixing and entrainment has also been achieved through numerical investigations. In an investigation of nearfield jet entrainment, Pergament and Dash [20] solved the parabolic Navier-Stokes equations with an implicit finite-differencing method to model mixing processes in the nearfield shear layer region of moderately underexpanded jets. Use of the two-equation k-ε viscous model was shown to provide strong agreement with experimental data for nearfield jet entrainment.

Use of the k-ε turbulence model also provided accurate estimation of jet entrainment for an investigation of flow control conducted by Steffen et al. [21]. The flowfield resulting from rectangular and circular nozzles fitted with delta tabs was studied both experimentally and computationally. The computational model used a finite volume approach with an upwind convective scheme that was second order accurate. A mesh resolution of 400,000 cells within a flow domain that included outflow boundaries located 20D downstream and at a radial distance of 10D provided strong agreement to the experimental data.

The conclusions presented in these investigations of separated shear layers and entrainment provide the foundation for the present investigation of high speed jet impingement. The entrainment of fluid through a series of internal channels can provide adequate heat transfer within a deflector. Through implementation of the solution techniques developed in these previous studies, accurate prediction of the resulting flowfield was confirmed.

3 Computational Model and Governing Equations Used in This Investigation

The commercially-available software package FLUENT was used to complete this investigation of flows related to high speed jet impingement. Validation of the computational model was performed by modeling underexpanded free jets as well as the impingement of underexpanded jets onto circular disks similar to the experimental tests conducted by Donaldson and Snedeker [1]. The working fluid throughout this investigation was air. Therefore, a robust computational model capable of predicting the effects due to high speed, turbulent, viscous, compressible, and time-dependent phenomena was utilized. The FLUENT software was developed to provide comprehensive modeling capabilities for a wide range of flows. With the correct combination of solvers, viscous model, and discretization methods defined, accurate prediction of the high speed jet flow was achieved.

3.1 Conservation Equations

The Navier-Stokes equations describe the motion of fluids and form the foundation of fluid mechanics. These relationships were developed from conservation principles of mass, momentum, and energy. For computational models, an equation for the conservation of energy is required to account for compressibility effects. In order to account for the time-dependent behavior of underexpanded jets, the Reynolds-averaged Navier-Stokes (RANS) set of equations are employed. Reynolds-averaging reduces the amount of computational resources required by computing average flow quantities allowing for the entire range of turbulence scales to be modeled. Use of the RANS

equations also introduces additional parameters of Reynolds stresses that must be modeled in order to provide closure.

The governing equations used in the present investigation are the RANS as follows:

Continuity:

$$\frac{\partial \rho}{\partial t} + \frac{\partial}{\partial x_i}\left(\rho u_i\right) = 0 \tag{1}$$

Momentum:

$$\frac{\partial}{\partial t}\left(\rho u_i\right) + \frac{\partial}{\partial x_j}\left(\rho u_i u_j\right) = -\frac{\partial \rho}{\partial x_i} + \frac{\partial}{\partial x_j}\left[\mu\left(\frac{\partial u_i}{\partial x_j} + \frac{\partial u_j}{\partial x_i} - \frac{2}{3}\delta_{ij}\frac{\partial u_i}{\partial x_i}\right)\right] + \frac{\partial}{\partial x_j}\left(-\rho\overline{u_i' u_j'}\right) \tag{2}$$

These equations were implemented through the use of the pressure-based implicit solver. The pressure-based solver uses a segregated algorithm for solving the governing equations sequentially. Although the solution convergence may be slower than a coupled algorithm, the segregated algorithm efficiently uses CPU memory. Improved stability can also result from use of the segregated algorithm as in the study of high speed jet entrainment by Dash et al. [20].

3.2 Turbulence Model

In order to provide closure to the RANS set of equations, use of an additional model is required to incorporate the effects of turbulence. A wide range of closure models are provided by FLUENT, each specific to different types of fluid flow. The most direct method of modeling turbulence is through the use of two-equation models that solve transport equations for the turbulent kinetic energy and dissipation rate

independently. Many of the previous studies on the computational modeling of free jets and jet impingement [12, 14, 15, 16, 19] demonstrated successful use of a two equation k-ε viscous model. The k-ε model was able to accurately characterize the turbulent mixing layer associated with high speed jets. Following the success of these previous investigations, the k-ε viscous model was selected for the current investigation.

The k-ε models offered by FLUENT include the standard, renormalization group (RNG), and realizable models. For each of these versions it is assumed that the flow is fully turbulent. Although the standard and RNG k-ε models have been used successfully for high speed and swirling flows, the realizable k-ε model has shown considerable advantages for modeling impinging flows. The realizable model was used by Moore and Moore [22] in their investigation of flows approaching the leading edge of a body and impinging on a flat plate. With improved formulation of the turbulent viscosity and an improved transport equation for the dissipation rate, the realizable k-ε viscous model has shown improvements for flows involving rotation, separation, and recirculation. In the CFD validation cases of free jets presented in Chapter 4 of this document, the realizable k-ε viscous model provided best agreement with experimental results of Donaldson and Snedeker [1]. The realizable k- ε viscous model equations are summarized in the following equations.

Turbulent Kinetic Energy:

$$\frac{\partial}{\partial t}(\rho k)+\frac{\partial}{\partial x_j}\left(\rho k u_j\right)=\frac{\partial}{\partial x_j}\left[\left(\mu+\frac{\mu_t}{\sigma_k}\right)\frac{\partial k}{\partial x_j}\right]+G_k-\rho\varepsilon-Y_M+S_k \qquad (3)$$

Dissipation:

$$\frac{\partial}{\partial t}\left(\rho\varepsilon\right)+\frac{\partial}{\partial x_j}\left(\rho\varepsilon u_j\right)=\frac{\partial}{\partial x_j}\left[\left(\mu+\frac{\mu_t}{\sigma_\varepsilon}\right)\frac{\partial \varepsilon}{\partial x_j}\right]+\rho C_1 S\varepsilon-\rho C_2\frac{\varepsilon^2}{k+\sqrt{\nu\varepsilon}}+S_\varepsilon \qquad (4)$$

3.3 Computational Grid

Formation of the computational grid receives considerable attention when conducting a computational analysis. Grid resolution must be high enough to accurately resolve gradients. However, CPU memory imposes a limit on the size and resolution of the grid used. Inaccuracies and long solution times can result if the grid is not formed correctly. Therefore, it is essential that a well developed grid be created for each specific study of interest.

Unstructured grids are useful for analyzing flows involving complex geometries. Unlike structured grids that require cell faces to be perpendicular to the flow direction, unstructured grids provide improved stability for swirling and turbulent flows. Due to the complex flow structure involved with the analysis of high speed jet impingement, an unstructured mesh composed of tetrahedral elements was used in this investigation. After the solution space was defined, it was subdivided into smaller volumes. This allowed for greater control of the mesh resolution. The mesh resolution required to obtain an accurate and steady solution was determined through a series of axisymmetric free jet investigations. The computational grids used throughout this investigation were created with the commercial software package GAMBIT.

After a steady solution was obtained, grid adaption techniques were used to further refine the computational grid in regions of high gradients. Grid adaption techniques were introduced in the early 1980s as a method of improving numerical solutions while minimizing the total number of mesh cells required for spatial accuracy. Rausch et al. [23] developed methods for applying grid adaption to unstructured grids for the analysis of steady and unsteady flows over NACA airfoils. Their results showed a

dramatic improvement in resolving shocks developed on the leading edge of an airfoil. Similarly, the investigations of vortex shedding conducted by Holmes and Connell [24] showed improved solutions when using grid adaption techniques on unstructured meshes.

A similar approach to the adaption techniques developed by Rausch et al. [23] was used with FLUENT in the current study. The computational grid was adapted to gradients of turbulence intensity in order to ensure high resolution in the region of separated shear layers. For the specified solution variable, the Euclidean norm of the gradient was multiplied by a characteristic length scale. The result is a volume weighted approach that takes the following form.

$$\left|e_{i1}\right| = \left(A_{cell}\right)^{\frac{r}{2}} \left|\nabla f\right| \tag{6}$$

The method used by FLUENT to formulate the gradients is also heavily dependent on the type of grid used. The study conducted by Holmes and Connell [24] on the use of unstructured grids provides insight on the use of cell based and node based methods of gradient formulation. The node based method computes the gradients from the weighted average of the cell values surrounding the nodes. The node based averaging of an unspecified parameter is presented in the following equation.

$$\bar{\phi}_f = \frac{1}{N_f} \sum_{n}^{N_f} \bar{\phi}_n \tag{7}$$

Holmes and Connell [24] demonstrated that this method of node based averaging on unstructured meshed provided better agreement to experimental data as apposed to

cell based averaging on unstructured meshes. For the 3-D tetrahedral mesh used in this investigation, the Green-Gauss node based method of gradient formulation was specified.

3.4 Discretization

The method used to discretize the governing equations over the computational grid can have a significant effect on the accuracy of the solution. The type of flow under consideration, in addition to whether a structured or unstructured grid is used, are both driving forces for the optimal choice of discretization method used. For this investigation, an unstructured grid provides the flexibility to achieve the high resolution required to resolve the separated shear layer on the deflector surface. As a result, the discretization scheme implemented by FLUENT must be able to resolve the high gradients and turbulent mixing of the high speed jet impingement.

Development of early upwind schemes used cell averaged data to obtain a solution and were normally applied to structured grids. The necessity to address such issues related to the effects of using structured and unstructured grids motivated the research of Barth et al. [25]. In their computational investigation of inviscid flow over a 3 element airfoil, an improved solution was obtained when using a higher order upwind scheme they developed for smoothly varying meshes.

The second-order upwind scheme that FLUENT provides computes the values at cell faces through averaging over the entire upstream cell, relative to the direction of the normal velocity. The second order accurate upwind scheme uses a Taylor series expansion of the cell-centered solution about the cell centroid to define values at the cell faces. This formulation requires that the determination of gradients in each upstream cell. Parameters are solved using the following expression.

$$\phi_{f,SOU} = \phi + \nabla\phi \cdot \vec{r} \tag{8}$$

3.5 Parallel Performance

For all parallel computations, there is a limit on the performance of the cluster related to the number of processors used. This upper limit is dependent on the type of computations, the parallel network of processors, and the total number of processors used in parallel. In order to asses the performance of the Anantham cluster, an investigation of the optimal number of parallel compute nodes was conducted. The time to complete 1,000 iterations of a computational model used to analyze a 3-D subsonic free jet was quantified for a parallel system composed of 10 to 80 processors in increments of 10 processors. The resulting compute times and corresponding number of processors are summarized in Table 3.1. A log-log plot of compute time versus number of processors is provided in Figure 3.1 and demonstrates the speedup characteristic for FLUENT. By comparing the actual and perfect speedup characteristics, the gains and limits associated with the parallel system were observed. From this investigation, it was determined that the optimal number of processors for executing parallel computations on the Anantham cluster is approximately 40. However, from the plot of the speedup characteristic, it was observed that very little is gained when increasing from 20 to 30 nodes. For the remaining CFD investigations performed on the Anantham cluster, it is suggested that the maximum number of processors be limited to approximately 40.

Table 3.1. Summary of compute time and corresponding number of processors used to complete 1,000 iterations of a 3-D subsonic jet computational model.

# of Processors	Compute Time (s)
80	6307.2
70	5725.3
60	4806.2
50	4366.8
40	4022.1
30	4158.9
20	4294.4
10	6402.3

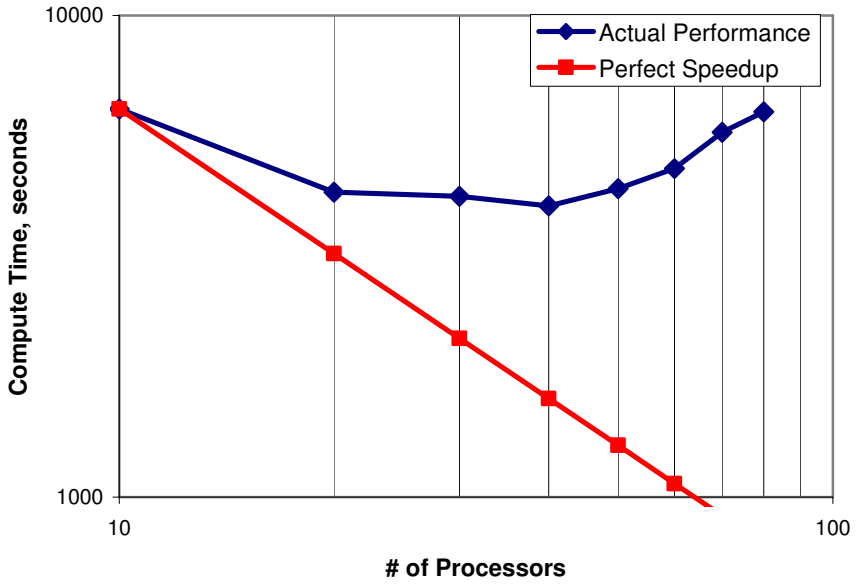

Figure 3.1. Log-log plot of FLUENT's speedup characteristic.

4 Results and Discussion

4.1 Review of Jet Flows Under Consideration

An extensive amount of research has been conducted on free jets. Experimental data is available for a vast range of flow conditions from laminar subsonic jets to highly compressible supersonic jets. The current investigation focused on three types of jet flow. These included a subsonic jet, moderately underexpanded jet, and a highly underexpanded jet. The inlet boundary conditions for each of these are presented in Table 4.1. There are distinct flow characteristics associated with each of these flows, which will be used to assess the accuracy of the computational model.

Table 4.1. Inlet boundary conditions for the three main jet flows investigated.

	Subsonic	Moderately Underexpanded	Highly Underexpanded
p_∞/p_0	0.80	0.372	0.148
p_1/p_∞	1.00	1.42	3.57
M_1	0.57	1.00	1.00

A subsonic jet issuing from a circular nozzle into quiescent air was first investigated. The subsonic jet is characterized by a potential core region that is surrounded by a mixing region. At a distance several nozzle diameters downstream of the nozzle exit, the mixing region spreads until there is no longer a potential core. The mixing region then continues to spread as the velocity of the jet decreases. A diagram of the subsonic jet flowfield is presented in Figure 4.1.

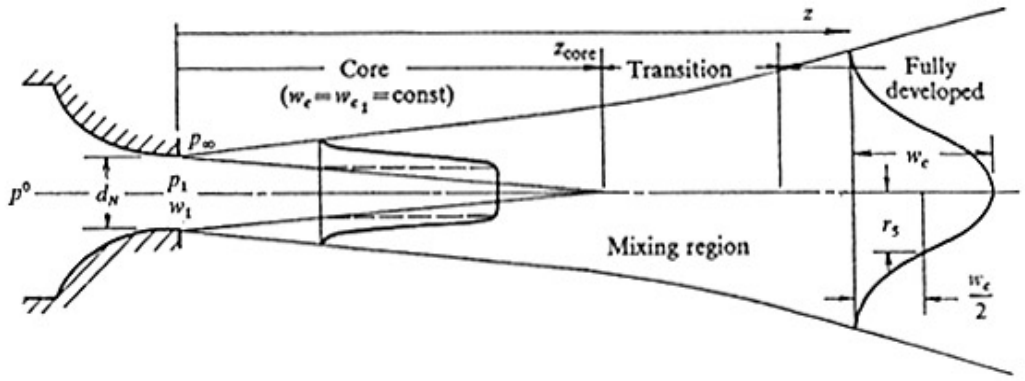

Figure 4.1. Flow structure corresponding to a subsonic jet.

The flow corresponding to the moderately underexpanded jet is significantly more complex than for the subsonic jet. An underexpanded jet is one in which the nozzle exit pressure is greater than the pressure of the atmosphere the jet is exhausting into. The term moderately underexpanded is used to denote jets with a nozzle outlet pressure ratio of $1.1 < p_1/p_\infty < 2$. Once the critical pressure at the nozzle outlet is reached, the formation of a normal shock is observed. As the pressure ratio increases, the formation of a reflecting shock pattern or "shock cells" are observed within the core of the jet. As the core region dissipates, the jet becomes subsonic and similar characteristics of a subsonic jet can be viewed. A diagram of the moderately underexpanded jet is provided in Figure 4.2.

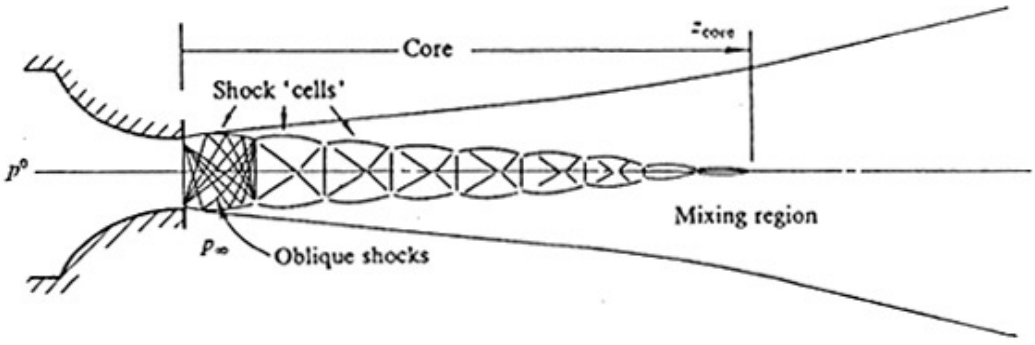

Figure 4.2. Flow structure corresponding to a moderately underexpanded jet.

As the nozzle outlet pressure ratio begins to increase, the reflecting shocks are no longer observed. For pressure ratios greater than two, recompression of the jet takes place through a large normal shock disk developed immediately downstream of the nozzle exit. Once this disk forms, the jet is said to be highly underexpanded. For very high pressure ratios, the region directly downstream of the shock disk is subsonic. A diagram of the highly underexpanded jet is provided in Figure 4.3.

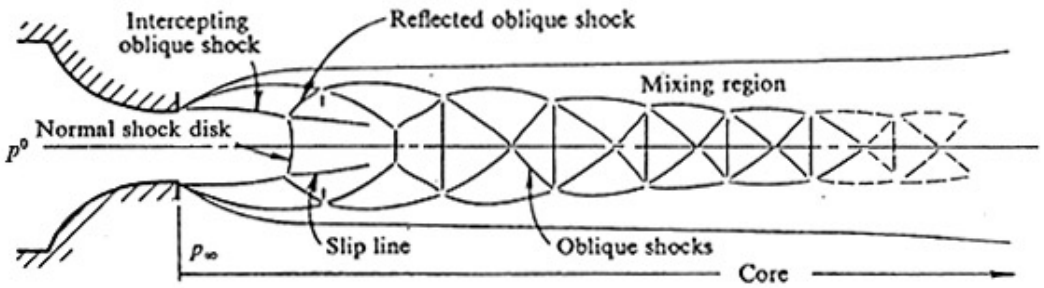

Figure 4.3. Flow structure corresponding to a highly underexpanded jet.

4.2 Computational Investigation of High Speed Flows

The development of the present computational model for the analysis of high speed jet impingement on deflectors was organized to follow the available experimental data. The following sections describe the several cases modeled, and provide a comparison of the CFD predictions with the experimental measurements.

FLUENT's ability to accurately model the flow field associated with several models of underexpanded jets was assessed. This was accomplished through an investigation of free jets issuing from circular nozzles. Inlet boundary conditions were specified according to the experimental setup used by Donaldson and Snedeker [1] in their investigation of free jet impingement. Three variations of jet flow were modeled

including a subsonic jet, moderately underexpanded jet, and a highly underexpanded jet. Both axisymmetric and full 3-D models were used to characterize the resulting flowfields. After development of the free jet model was complete, the flow field resulting from free jet impingement was also investigated. The experimental data collected by Donaldson and Snedeker [1] on the impingement of a moderately underexpanded jet provided the necessary data to validate results obtained from the computational model.

4.3 Axisymmetric Free Jet Investigation

Development of the numerical model began with an axisymmetric analysis of free jet flows. Flowfields were predicted for various inlet conditions corresponding to the experiments performed by Donaldson and Snedeker [1]. Non-dimensional velocity profile data was collected at locations of 1.96m, 3.92m, 7.32m, and 11.7m downstream of the nozzle. These axisymmetric cases provided a method to quickly observe what combination of viscous model and algorithms resulted in the greatest accuracy and stability.

The solution space created for this investigation included a simple convergent round nozzle in order to achieve the jet flow Mach number and pressure ratios desired. The grid was composed of a 1.0m length inlet boundary that converged to a throat of 0.5m. Pressure outlet boundaries were positioned 15m downstream of the inlet and at a radial distance of 7m from the symmetry axis. The mesh used for the free jet analyses is shown in Figure 4.4. An unstructured mesh was applied to the flowfield with an initial resolution of approximately 200,000 tetrahedral cells. For each of the CFD cases

presented below, grid independence was confirmed by increasing the resolution through grid adaption techniques up to 400,000 cells. By applying grid adaption techniques to a converged solution, the resolution required to accurately resolve the turbulent boundary layer was determined.

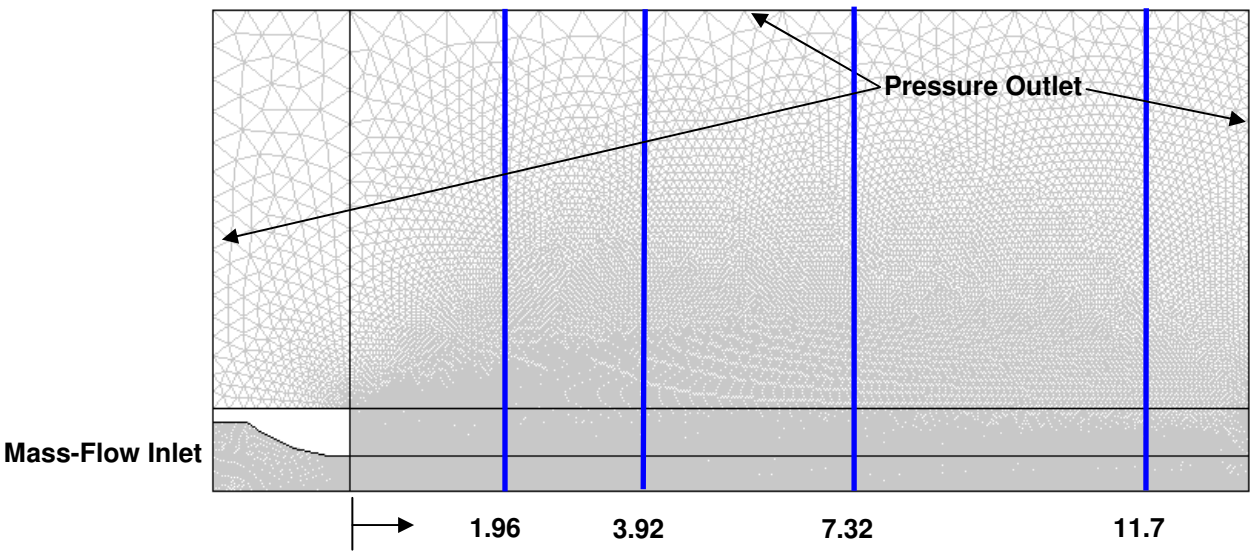

Figure 4.4. Schematic of the flow field geometry and boundary conditions used for the axisymmetric validation cases of a high speed jet.

4.3.1 Subsonic Jet

To achieve the Mach 0.57 flow for the first validation case, a mass-flow-inlet boundary condition was applied to the 2m diameter nozzle inlet($_o$). By then applying standard atmospheric conditions to the outlet boundaries($_\infty$), the desired inlet pressure ratio (p_∞/p_o) was achieved along with desired conditions at the throat of the nozzle($_1$). A mass flowrate of 405.65 lbm/s applied to the inlet boundary produced a pressure ratio of 1.0 and a Mach number of 0.568. Non-dimensional velocity data was calculated at various positions along the axis of symmetry and is presented in Figure 4.5. For the plots

of computational and experimental values, the parameter r_5 is used to non-dimensionalize the radius values. Parameter r_5 corresponds to the radial position where the flow speed is half of the maximum flow speed for each specific axial position. A comparison of the computational and experimental data for the Mach 0.57 flow is provided in Figure 4.6. The percent error associated with the computational model was computed for each velocity profile. As shown, the CFD predictions agree quite well with the experimental data. The viscous model that provided the best agreement was found to be the realizable k-ε model. After a converged solution was obtained, the grid was adapted to gradients of turbulence intensity in order to improve the resolution of the grid within regions of high gradients. The data presented below was obtained with a grid resolution of approximately 300,000 cells.

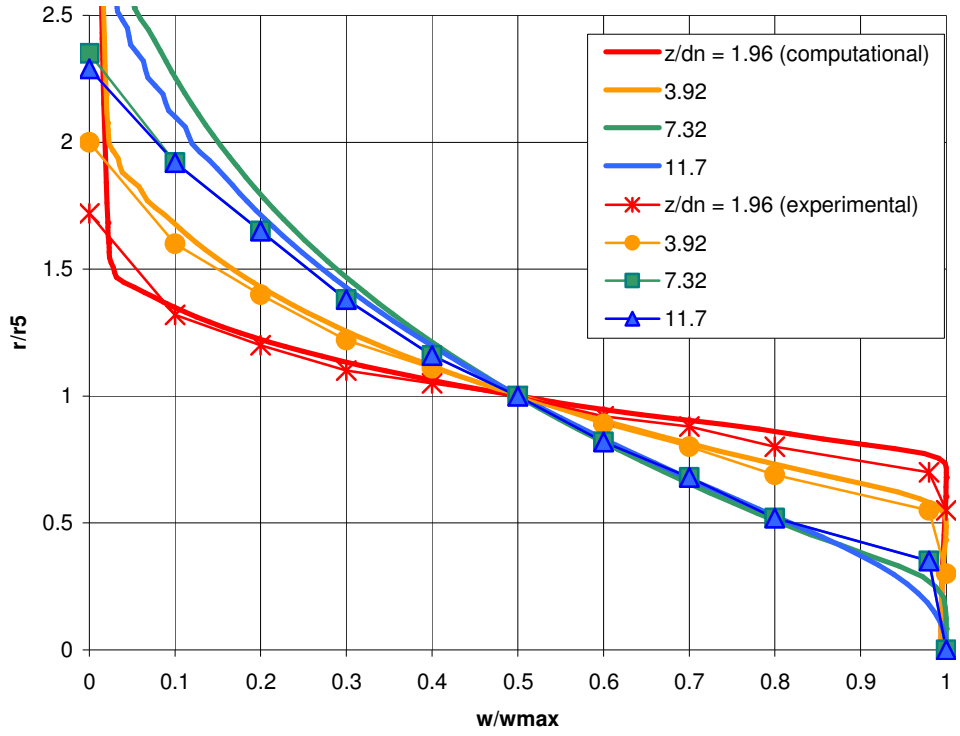

Figure 4.5. Computational and experimental data for the axisymmetric subsonic free jet.

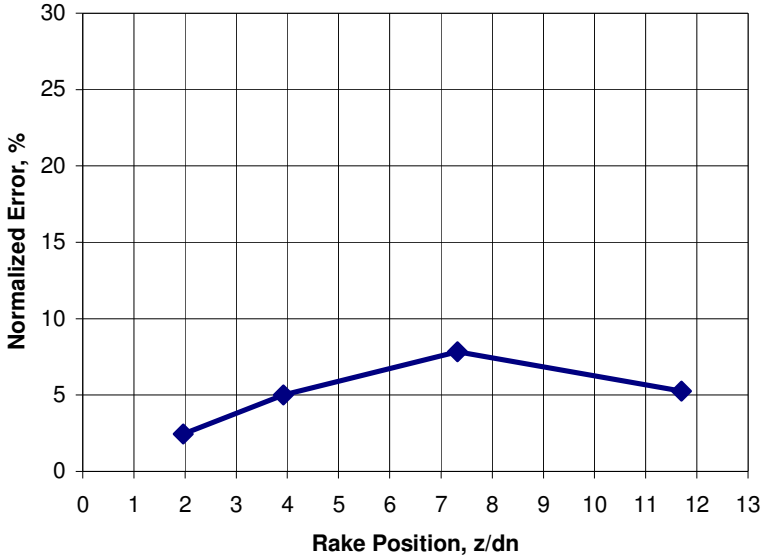

Figure 4.6. Normalized error associated with the prediction of a subsonic free jet with an axisyemmetric computational model.

4.3.2 Moderately Underexpanded Jet

In order to predict the nozzle exit conditions of the moderately underexpanded jet, it was necessary to define a pressure inlet boundary at the nozzle inlet. This allowed for greater control and ensured that the desired pressure ratio of 1.42 was reached. The convergent nozzle used in these trials ensured that a flow Mach number of 1.0 was maintained at the throat. Through these specifications, inlet conditions used in the experimental setup used by Donaldson and Snedeker [1] were achieved.

Velocity profiles obtained from the computational model and experimental setup are provided in Figure 4.7. The plot of percent error values presented in Figure 4.8 represents the ability of an axisymmetric FLUENT model to predict the flowfield of an underexpanded jet. As with the subsonic jet case, the realizable k-ε viscous model provided the best prediction of the resulting jet. By adapting the grid to gradients of turbulent intensity, the formation of reflecting shocks downstream of the nozzle was

resolved. However, large inconsistencies were observed in regions farthest from the center of the jet.

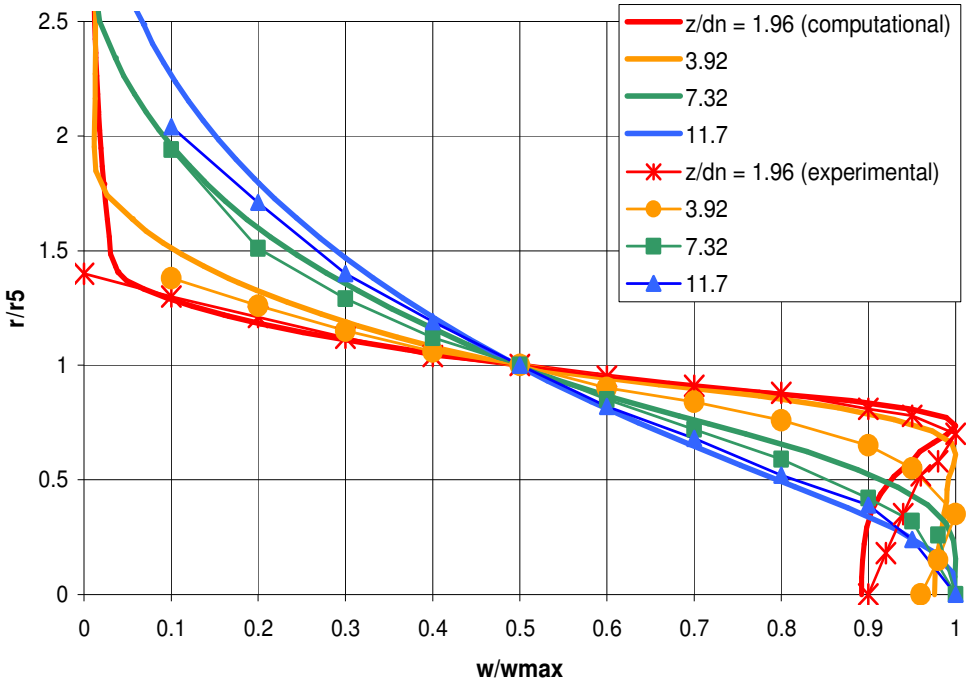

Figure 4.7. Computational and experimental data for the axisymmetric moderately underexpanded jet.

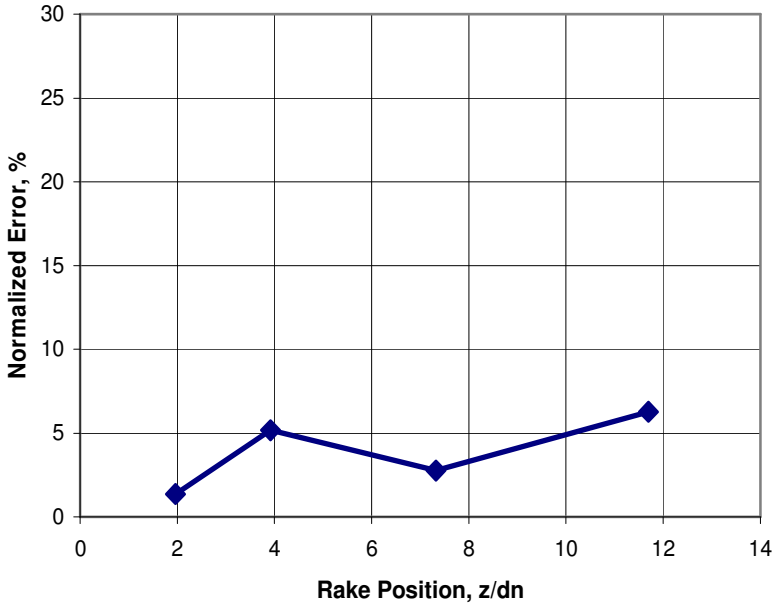

Figure 4.8. Normalized error associated with the prediction of a moderately underexpanded free jet with an axisymmetric computational model.

4.3.3 Highly Underexpanded Jet

Solutions obtained for the axisymmetric subsonic and moderately underexpanded jets agreed very well with experimental data. However, as the pressure ratio increased to 3.57, the accuracy of the CFD model for predicting the central jet core flow diminished. Increasing the resolution of the computational grid showed little improvement. The resulting velocity contours and error plots presented in Figures 4.9 and 4.10 demonstrate errors in the prediction of the flow directly downstream of the nozzle exit.

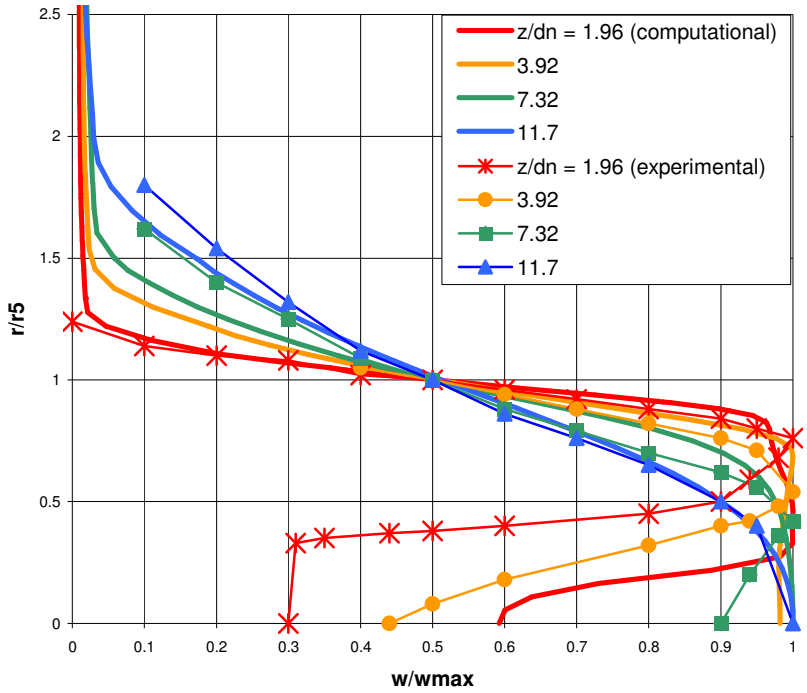

Figure 4.9. Computational and experimental data for the axisymmetric highly underexpanded jet.

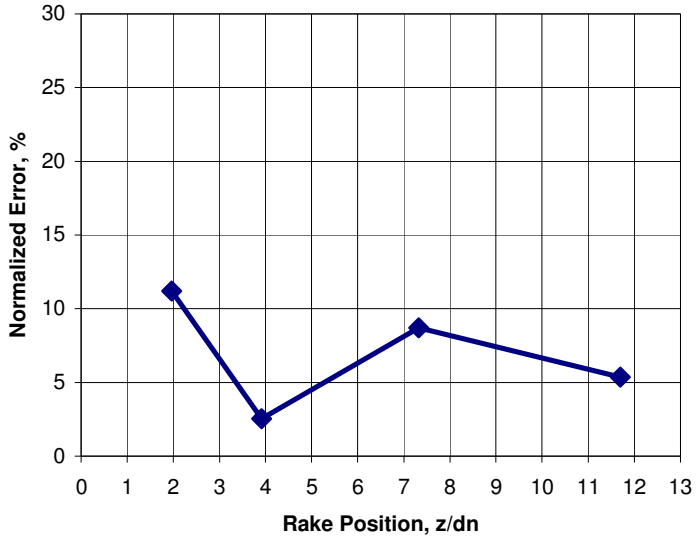

Figure 4.10. Normalized error associated with the prediction of a highly underexpanded free jet with an axisymmetric computational model.

There are several factors that are known to contribute to inconsistencies found in the modeling of the highly underexpanded jet. In their investigation of free and impinging jets, Donaldson and Snedeker [1] mention several issues that affected their profile measurements. They first mention the formation of a flapping instability. This is a low frequency lateral oscillation of the entire flow field that all turbulent jets experience. This flapping has an immediate effect on the spreading and decay rates of the jet. In addition, measurements taken with pitot and static pressure probes are subject to error due to the turbulence of the jet. This has a direct effect on the velocity profile measurements. Donaldson and Snedeker admit that accuracy of their measurements is greatest in regions of the jet where turbulence is small relative to the mean flow velocity.

In addition to the error associated with the experimental data, an unknown amount of error was introduced with the extraction of data points from the figures provided in the published report. A complete set of experimental data was not provided for this

investigation. In regions where experimental data was not available, extrapolation of the corresponding values was necessary.

Normalized error plots created for each of the flows predicted by the axisymmetric model demonstrate agreement to experimental results within 10%. After confirming that an axisymmetric FLUENT model can be used to predict underexpanded free jets, the solution techniques used in these cases were applied to a 3-D computational model. Through the development of a 3-D model, the solution controls necessary to ensure a stable solution will be determined. The resulting computational model can then be used to investigate impinging jets.

4.4 Full 3-D Free Jet Investigation

By performing computations of high speed jet flow with an axis-symmetric model, the combination of solvers and algorithms that produced the most accurate prediction of the resulting flow field were obtained. The system of equations used for this computational model were then applied to the 3-D validation of a jet exhausting into quiescent air. The three jet flow conditions analyzed with the axisymmetric model were once again investigated. Velocity profile data was collected at locations of 1.96m, 3.92m, 7.32m, and 11.7m downstream of the nozzle exit were compared to the experimental results obtained by Donaldson and Snedeker. Validation of this computational model confirms the ability of FLUENT to accurately predict the full 3-D flow field associated with underexpanded jets.

The 3-D solution space used in this analysis was created by revolving the edges of the axisymmetric model around the center axis. The result was a solution domain that

includes a 2m diameter inlet boundary converging to a throat diameter of 1m within a cylinder with a diameter of 14m and a length of 15m. As before, a mass flow inlet boundary was initially applied to the nozzle inlet and an outlet pressure boundary was applied to the entire surroundings. A model of the solution space along with the resulting mesh is provided in Figure 4.11. An unstructured 3-D grid of tetrahedral elements was applied to the domain producing a resolution of 1,200,000 cells. After grid adaption techniques were applied to regions of high gradients, resolutions of approximately 2,000,000 cells were obtained. The realizable k-ε viscous model in combination with the 2^{nd} order accurate, segregated, implicit solver were specified in order to ensure accuracy and stability. By performing the computations on the Anantham cluster, the time required to obtain a solution was drastically improved.

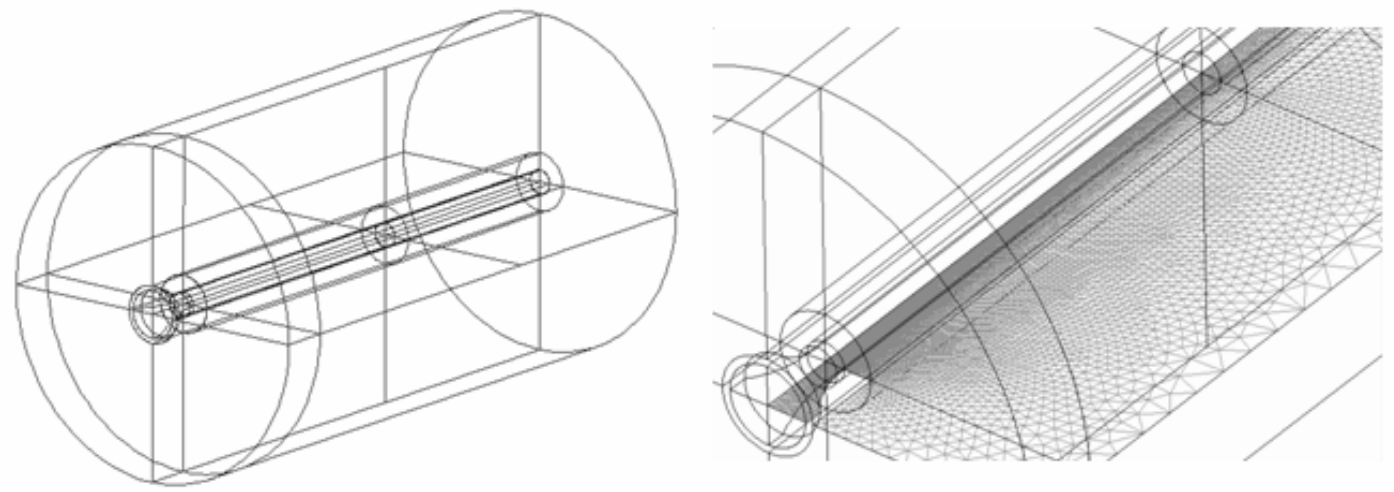

Figure 4.11. 3-D computational grid used to investigate a free jet.

4.4.1 Subsonic Jet

Velocity profiles obtained downstream of the nozzle exit were compared to the experimental data obtained by Donaldson and Snedeker [1]. After multiple iterations of the computational grid arrangement, initial grid resolution, and flow initialization procedure were investigated, the correct combination of these variables required for an accurate and stable solution was determined. A mass flowrate of 405.65 lbm/s at atmospheric pressure was applied to the mass flow inlet boundary. This produced a pressure ratio of 1.0 and a Mach number of 0.568. As in the previous cases, atmospheric boundary conditions were applied to the pressure outlet boundaries. After a steady solution was obtained, grid adaption techniques were applied to the computational grid. Characterization of the resulting flowfield was then completed and the resulting velocity profiles were compared to experimental results. A plot of velocity contours provided in Figure 4.12 demonstrates the formation of the core, transition, and fully developed regions of the free jet. The velocity contours provide a visual check to investigate the decay and spreading rates associated with the high speed jet. A comparison of the velocity profile data obtained from the computational model is presented in Figure 4.13.

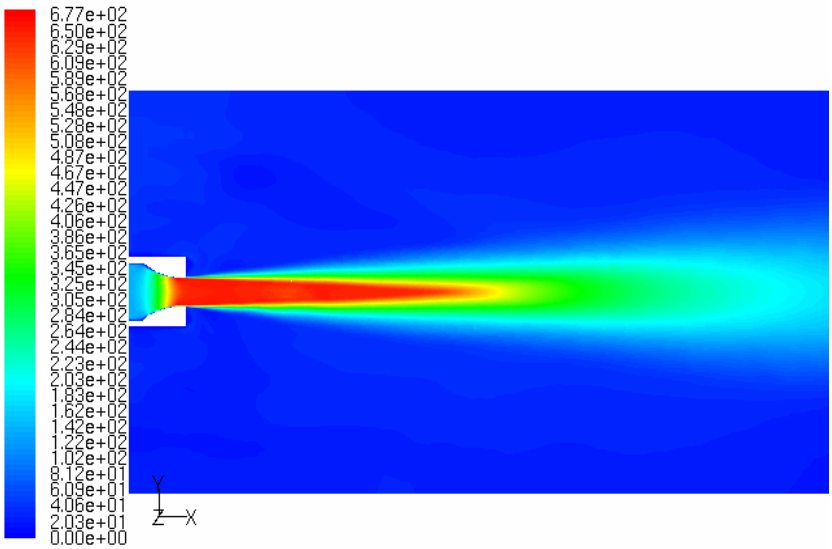

Figure 4.12. Velocity contours for the 3-D subsonic free jet.

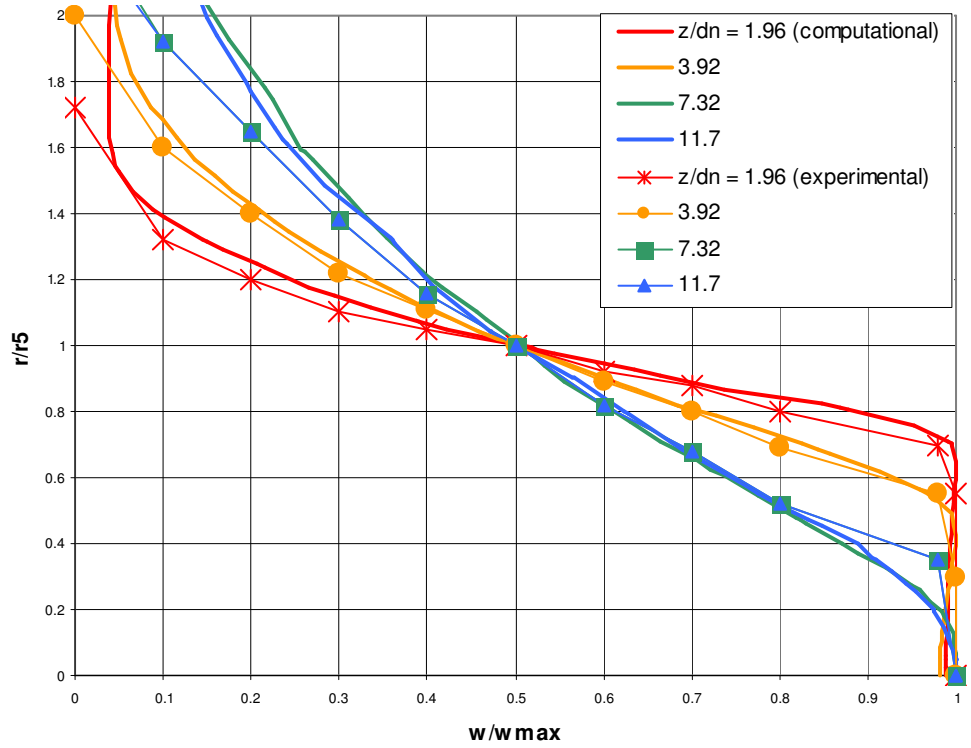

Figure 4.13. Computational and experimental data for the 3-D subsonic jet.

In order to assess the accuracy of the numerical solutions, plots of normalized error plots were created by extracting data points from figures presenting the experimental results obtained by Donaldson and Snedeker [1]. Normalized percent error

values were computed by dividing the sum of absolute values of the difference between experimental and computational data by the sum of reference experimental data points as follows:

$$\xi = \frac{\sum abs(\phi_e - \phi_c)}{\sum abs(\phi_e)} 100\% \tag{10}$$

The corresponding error plot for the subsonic jet is presented in Figure 4.14. It must be noted that there is an unknown level of uncertainty introduced in the percent error values due to the graphical extraction and the extrapolation of the experimental data points. The actual experimental values were not provided. Computed streamlines clearly show the entrainment of quiescent air into the jet. The velocity contours provide a visual check to investigate the decay and spreading rates associated with the high speed jet.

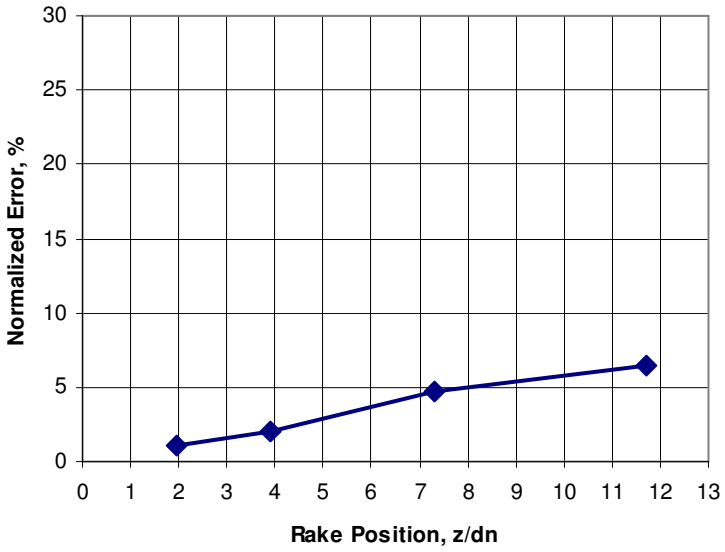

Figure 4.14. Normalized error associated with the velocity profiles obtained at various axial locations for the 3-D subsonic free jet.

4.4.2 Moderately Underexpanded Jet

To obtain a solution for a moderately underexpanded free jet, the pressure inlet condition was applied at the inlet boundary. This provided greater control of the resulting pressure ratio. An inlet pressure of 5716.8 psf was applied to inlet, which produced the underexpanded jet shown in Figure 4.15. In order to ensure a stable solution, the grid was adapted to gradients of turbulence intensity. The development of the reflecting shock pattern was very clear. Streamlines within the flow field were calculated, demonstrating the entrainment of air into the jet. Proper resolution was required to ensure that entrainment due to the turbulent mixing of the high speed jet and quiescent air was modeled correctly.

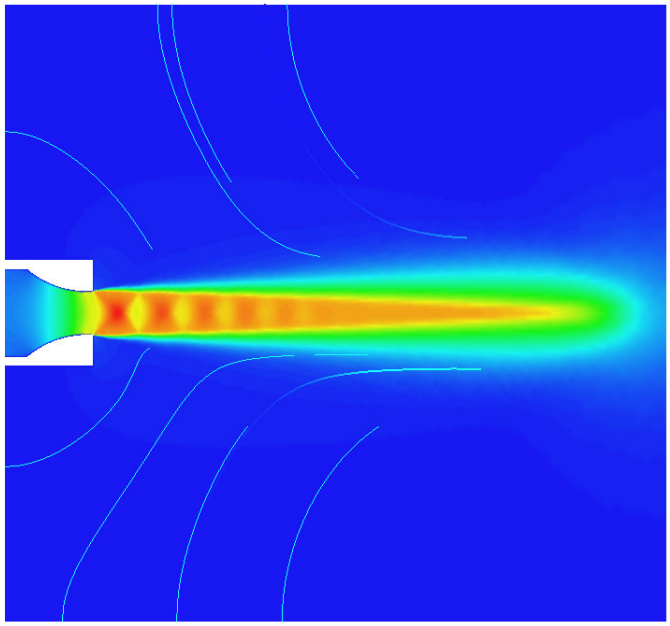

Figure 4.15. Velocity contours obtained for the 3-D moderately underexpanded free jet.

The resulting velocity profiles obtained from the computational flowfield were then compared to the experimental data obtained by Donaldson and Snedeker [1]. The

numerical and experimental velocity profile data is presented in Figure 4.16 along with the corresponding percent error values presented in Figure 4.17.

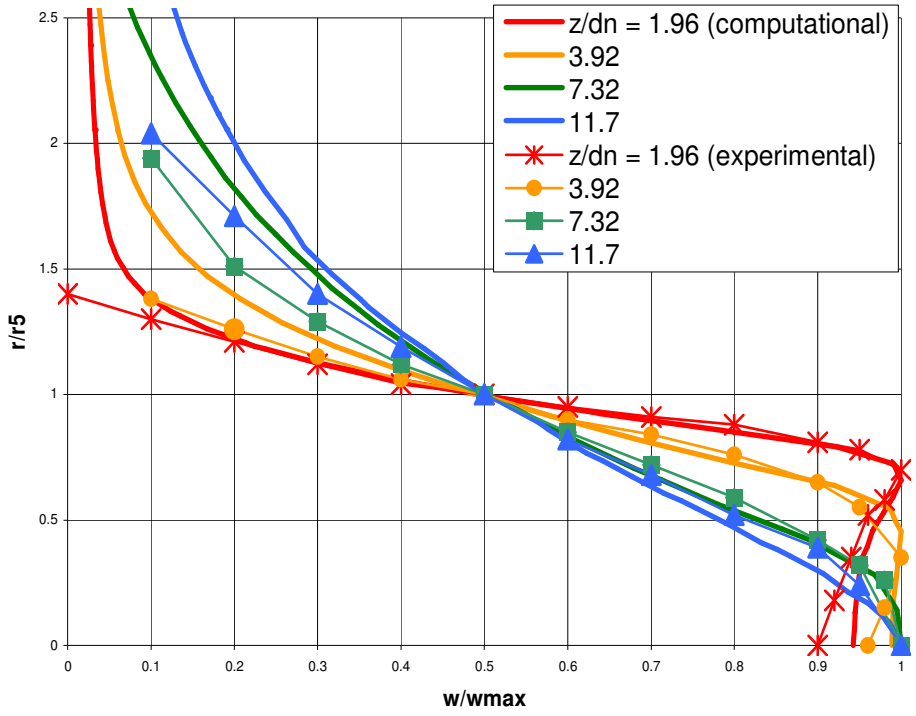

Figure 4.16. Computational and experimental results for the 3-D moderately underexpanded free jet.

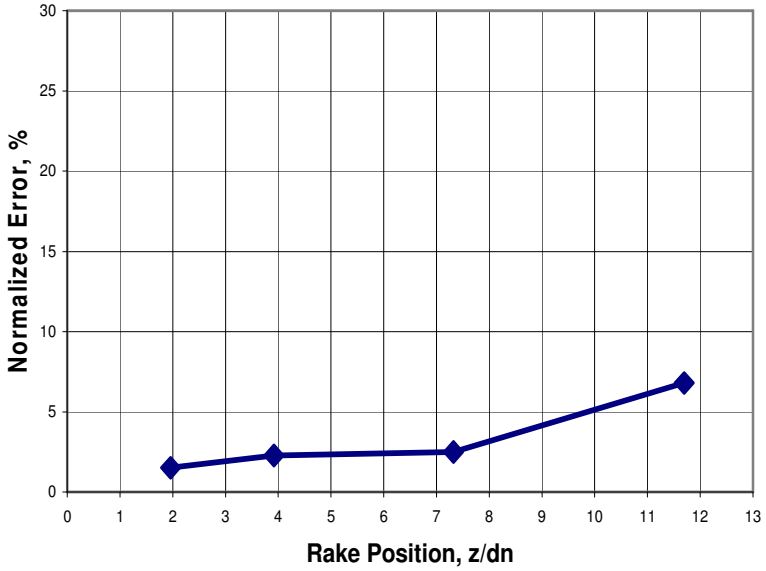

Figure 4.17. Normalized error associated with the velocity profiles obtained at various axial locations of the 3-D moderately underexpanded free jet

Use of the grid adaption technique greatly improved the convergence of the computational model. The resulting resolution of the computational grid was 2,180,000 cells. By using a ratio method to perform the grid adaption, regions of high gradients were resolved, while regions of very small gradients were coarsened. This ensured that the computations did not become too expensive. The reflecting shocks predicted by the computational model compare very well to the Schlieren photograph images taken by Donaldson and Snedeker as shown in Figure 4.18.

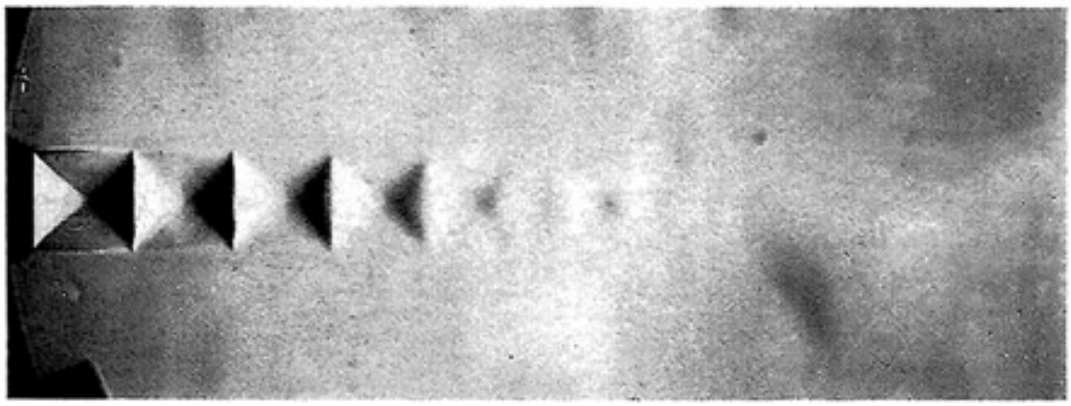

Figure 4.18. Schlieren photograph of the moderately underexpanded jet obtained through the experiments of Donaldson and Snedeker.

4.4.3 Highly Underexpanded Jet

Solutions obtained for the subsonic jet and moderately underexpanded jet cases showed very good agreement to experimental results. However, the highly underexpanded jet corresponding to a pressure ratio of 3.57 proved to be a significantly more challenging flow to model. After applying a considerable amount of refinement to the computational grid, a fully converged solution was not obtainable. By defining a nozzle inlet pressure of 14693 psf, the desired nozzle outlet conditions were reached, but

the resulting downstream flowfield would not develop. Divergence of the initial solution occurred due to the extremely high dissipation rates associated with the formation of the shock disk. Modifications to the computational model were necessary to fully characterize the flow.

In order to improve the stability of the downstream flow field, several techniques were implemented. Through the use of a low area ratio convergent-divergent nozzle, the jet is allowed to expand to a low supersonic Mach number. The flow is then pushed out of the nozzle after it is chocked at a Mach number of 1.00. A nozzle was created for an outlet Mach number of 1.10, which resulted in an area ratio (outlet area / throat area) of 1.008. The necessary inlet boundary conditions required to obtain the desired pressure ratio were determined from the analysis of an axis-symmetric model with inclusion of the same low area ratio nozzle. Velocity contours provided in Figure 4.19 were obtained for a full 3-D model for the analysis of the highly underexpanded jet with inclusion of the low area ratio nozzle. By applying a pressure of 14693psf at the inlet boundary, the desired flow conditions were achieved. A comparison of the computational solution to experimental data is provided in Figure 4.20 along with the corresponding error plots in Figure 4.21.

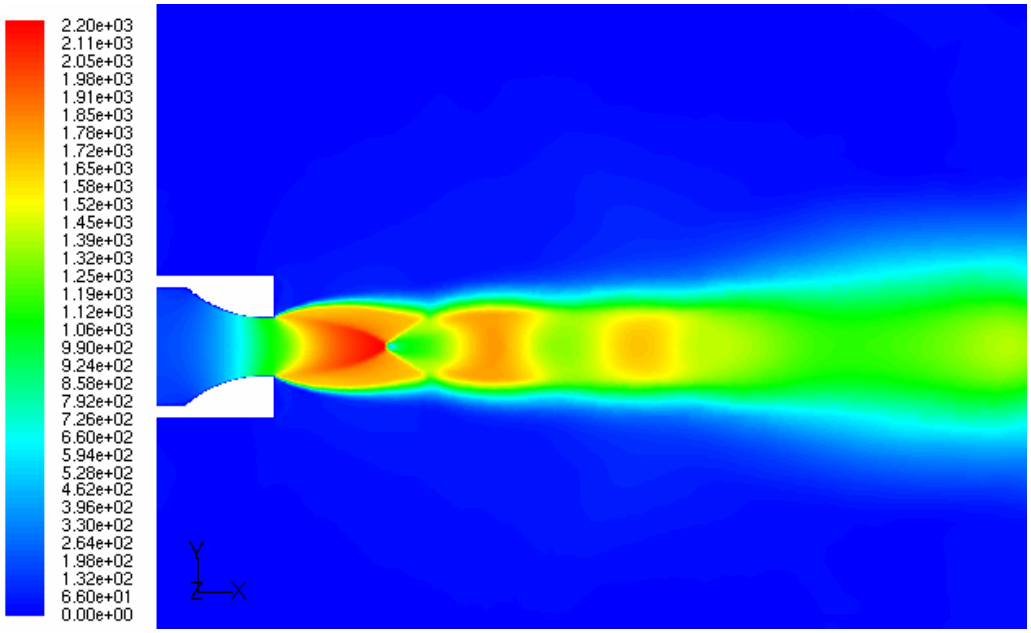

Figure 4.19. Velocity contours for the 3-D highly underexpanded free jet issuing from a convergent-divergent nozzle.

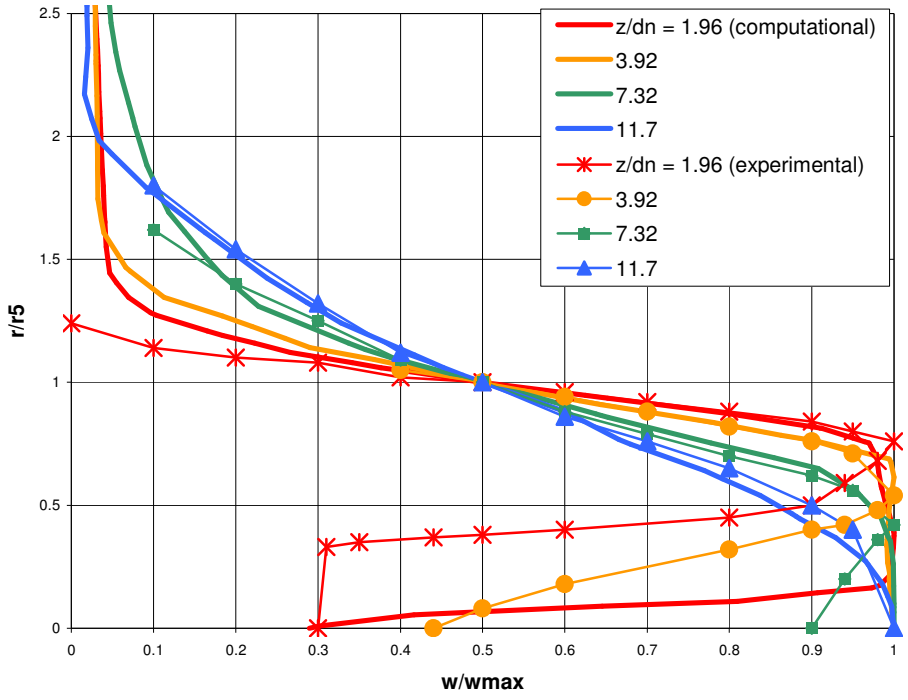

Figure 4.20. Computational and experimental results for the 3-D highly underexpanded free jet.

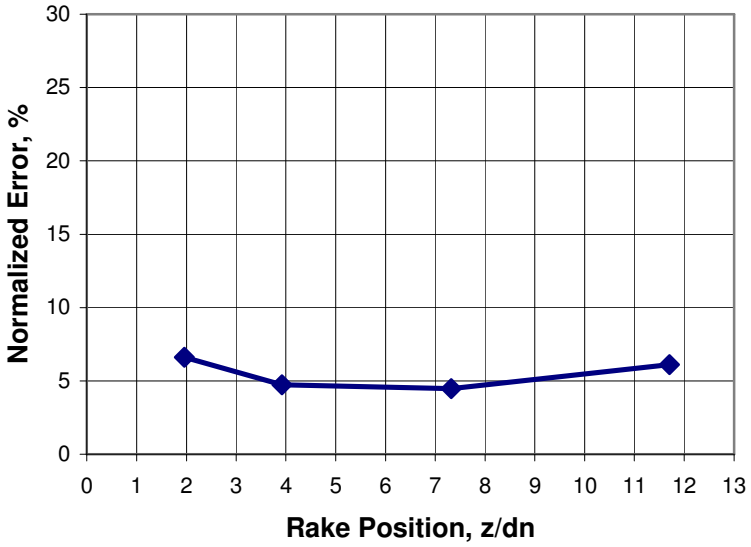

Figure 4.21. Normalized error associated with the velocity profiles obtained at various axial locations of the 3-D highly underexpanded free jet

Calculation of the percent error associated with the computational solution indicates that the spreading and decay rates predicted for the highly underexpanded jet are inaccurate. However, as with the other free jet cases analyzed, there is an unknown amount of error associated with the experiments due to the extrapolation of data points. It is recommended that further validation of the computational model to further experimental data be performed.

4.5 Impingement of a Moderately Underexpanded jet

Flowfields resulting from the impingement of high speed jets onto deflecting surfaces is of general interest. Flowfields corresponding to the impingement of underexpanded jets onto large disks were characterized by Donaldson and Snedeker [1]. Through there investigation, the entire flow within the free jet, impingement, and wall jet regions were characterized. A diagram of the experimental set up used in their

investigation is shown in Figure 4.22. Of considerable importance to the current investigation was the use of pitot tube rakes installed along the edge of the circular disk to obtain wall jet velocity profiles. Experiments were conducted to obtain wall jet profiles for disks at angles ranging from 90° to 45° relative to the jet center axis. For the current investigation, the flow fields corresponding to the impingement of a moderately underexpanded jet onto disks at angles of 60° and 45° were of significant importance. Through the validation of a computational model used to predict the impingement of an underexpanded jet, use of FLUENT to accurately predict the flow field resulting from the deflection of a high speed jet and the entrainment of quiescent air was confirmed.

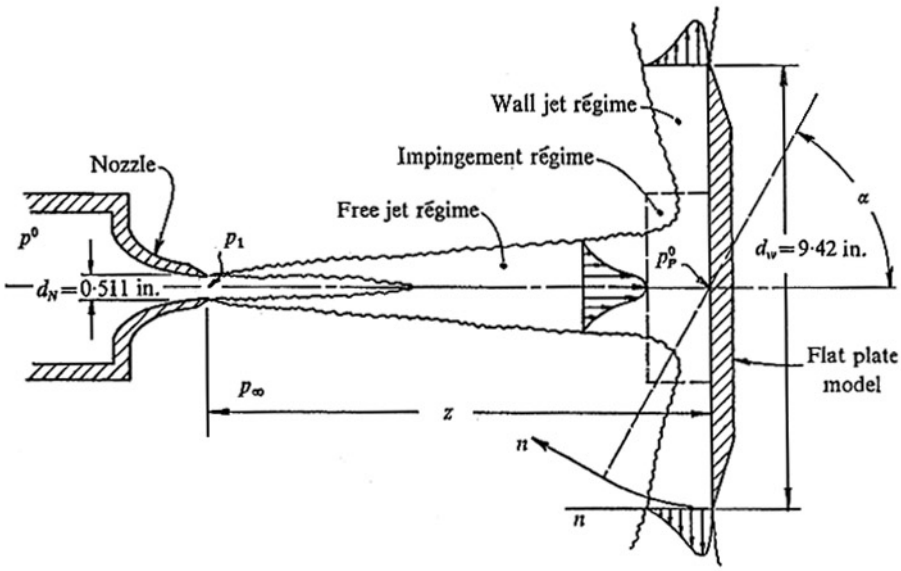

Figure 4.22. Diagram of the experimental setup used by Donaldson and Snedeker to investigate the impingement of underexpanded jets.

4.5.1 Impingement onto a 60° Disk

The first case investigated was the impingement of a moderately underexpanded jet onto a disk rotated 60° relative to the jet centerline axis. The 3-D solution space used for this validation was created according to the specifications of the

experimental setup presented by Donaldson and Snedeker [1]. Non-dimensional values for disk radius and axial location of the disk were given in relation to the nozzle outlet diameter. The simple convergent nozzle used in the previous solution was included in the computational domain for this case. The nozzle included an inlet boundary with a diameter of 2.0m and an outlet diameter of 1.0m. The corresponding disk was created with a diameter of 18.433m and was located 7.32m downstream of the nozzle exit. The surrounding outlet boundary was positioned at a radial distance of 20m from the center of the jet and at an axial distance of 20m from the inlet boundary. The solution space along with images of the initial mesh resolution for the 60º disk are presented in Figure 4.23.

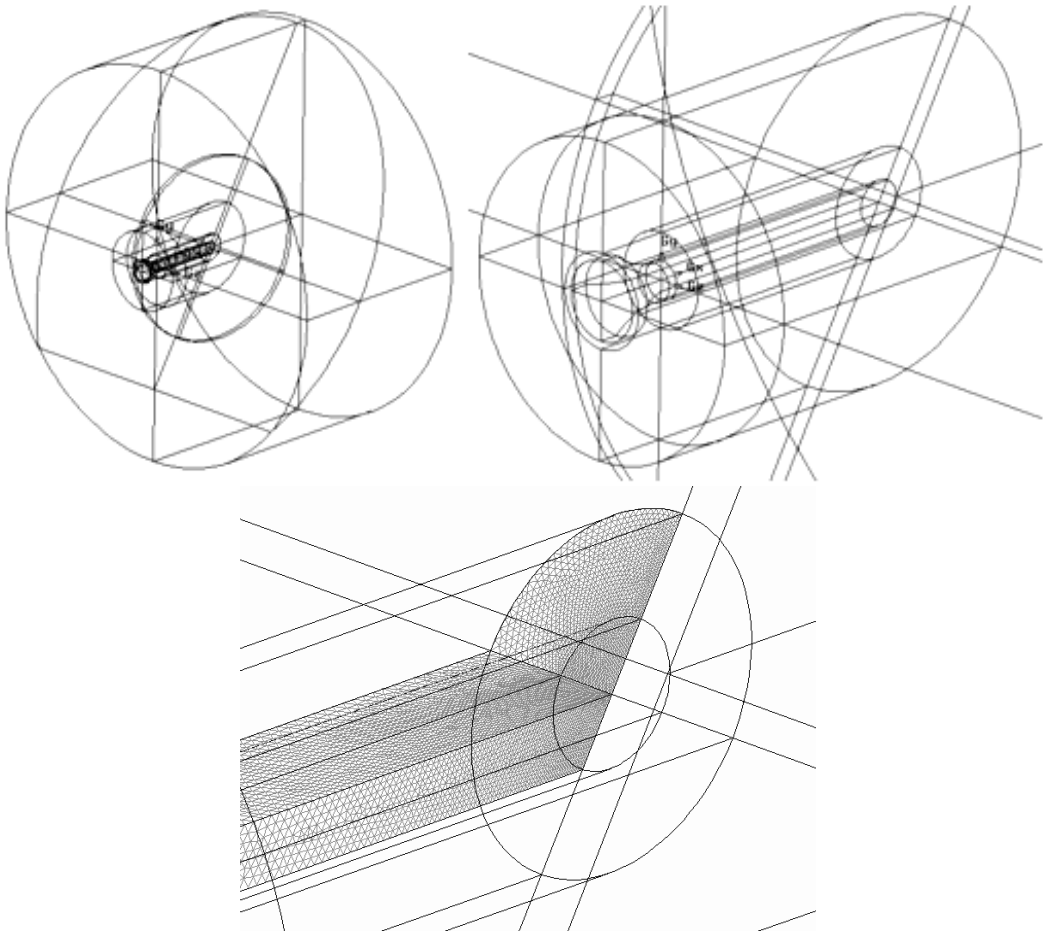

Figure 4.23. Solution space used to model the impingement of a moderately underexpanded jet disk at 60°.

An unstructured 3-D grid composed of tetrahedral cells was applied to the computational domain producing a resolution of 1,800,000 cells. After obtaining a steady solution, adaption of the grid to gradients of turbulence intensity ensured that a converged solution would be obtained. The resulting grid resolution was approximately 2,200,000 cells. Use of the realizable k-ε viscous model in combination with the 2nd order accurate, segregated, implicit solver provided a stable and accurate solution.

Formation of the moderately underexpanded jet was achieved by applying the same inlet conditions used for the free jet cases. Application of a nozzle inlet pressure of 5716.8 psf resulted in a Mach number of 1.0 and a pressure ratio of 1.42. Contours of velocity magnitude resulting from the impingement of the moderately underexpanded jet are provided in Figure 4.24. The formation of the reflecting shocks was observed as well as an increase of velocity within the core region just before impingement with the disk. Through the calculation of streamlines, it is observed that air is entrained into the jet exhaust as well as the suction of air along the backside of the disk. In order to validate the predicted flowfield, wall jet velocity profiles were obtained along the edge of the disk. A comparison of the numerical and experimental wall jet velocity profiles for this flow arrangement is provided in Figure 4.25.

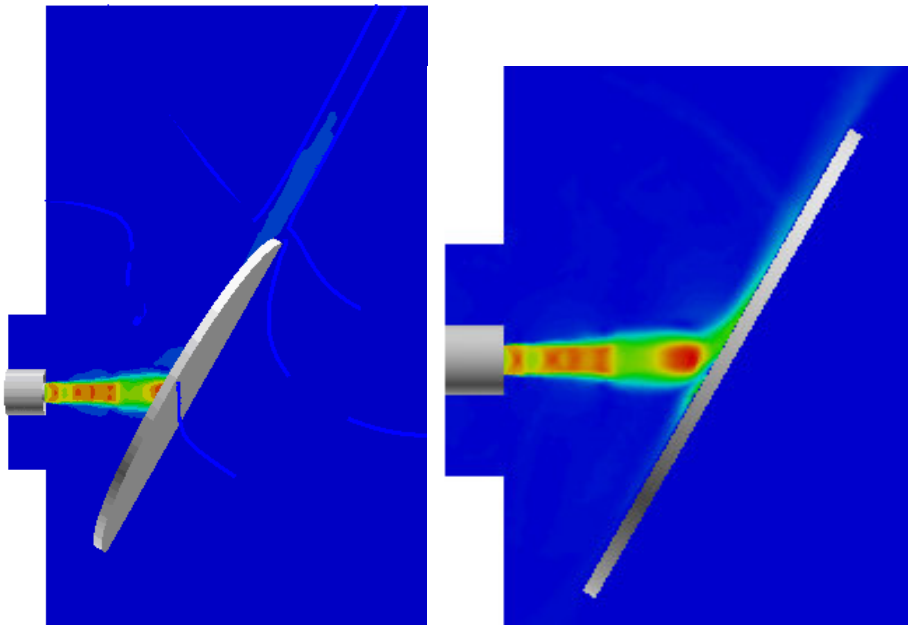

Figure 4.24. Velocity contours obtained for the impingement of a moderately underexpanded onto a 60° disk.

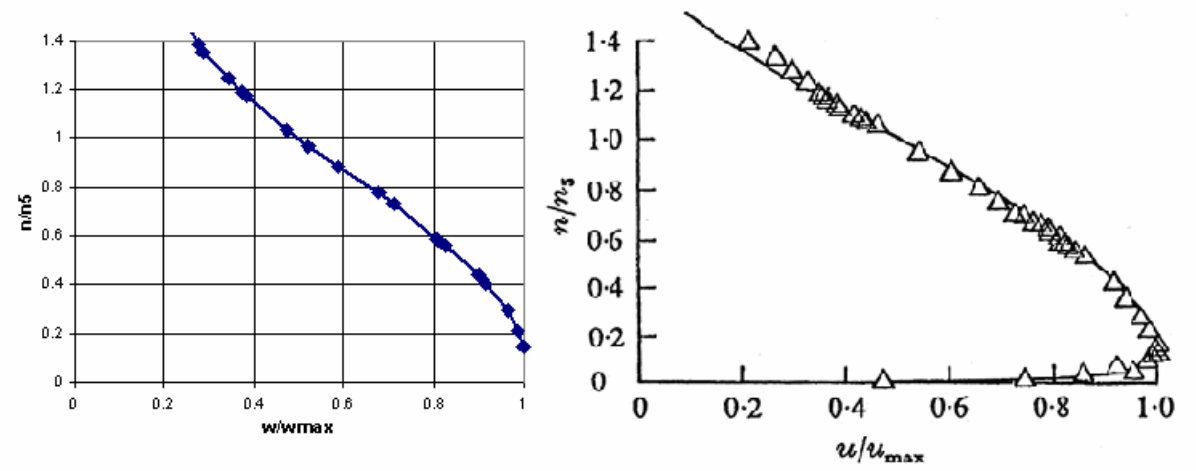

Figure 4.25. Computational (left) and experimental (right) wall jet velocity profiles for a moderately underexpanded jet impinging on a 60º disk. This velocity profile was obtained at the 12 o'clock position of the disk.

Wall jet velocity profiles obtained from the computational model were found to agree very well with the experimental data. Wall jet velocity profiles along the edge of the disk were obtained at intervals of 30°. For each of the profiles obtained, a lack of resolution within the viscous boundary layer of the wall jet was observed. Multiple

attempts to improve the resolution of the grid within this region resulted in a memory overload error. Further development of techniques to adapt the grid within the boundary layer on the surface of the disk is required to fully characterize the distribution of the impinging jet.

4.5.2 Impingement onto a 45° Disk

A similar procedure was used to predict the flowfield resulting from the impingement of a moderately underexpanded jet onto a disk rotated 45° from the axis of the jet. The simple convergent nozzle included an inlet boundary with a diameter of 2.0m with an outlet diameter of 1.0m. This resulted in a disk diameter of 18.433m located 7.32m downstream of the nozzle exit. The surrounding outlet boundary was positioned at a radial distance of 20m from the center of the jet and at an axial distance of 20m from the inlet boundary. The final solution space created along with the resulting mesh for the 45º angled disk are presented in Figure 4.26.

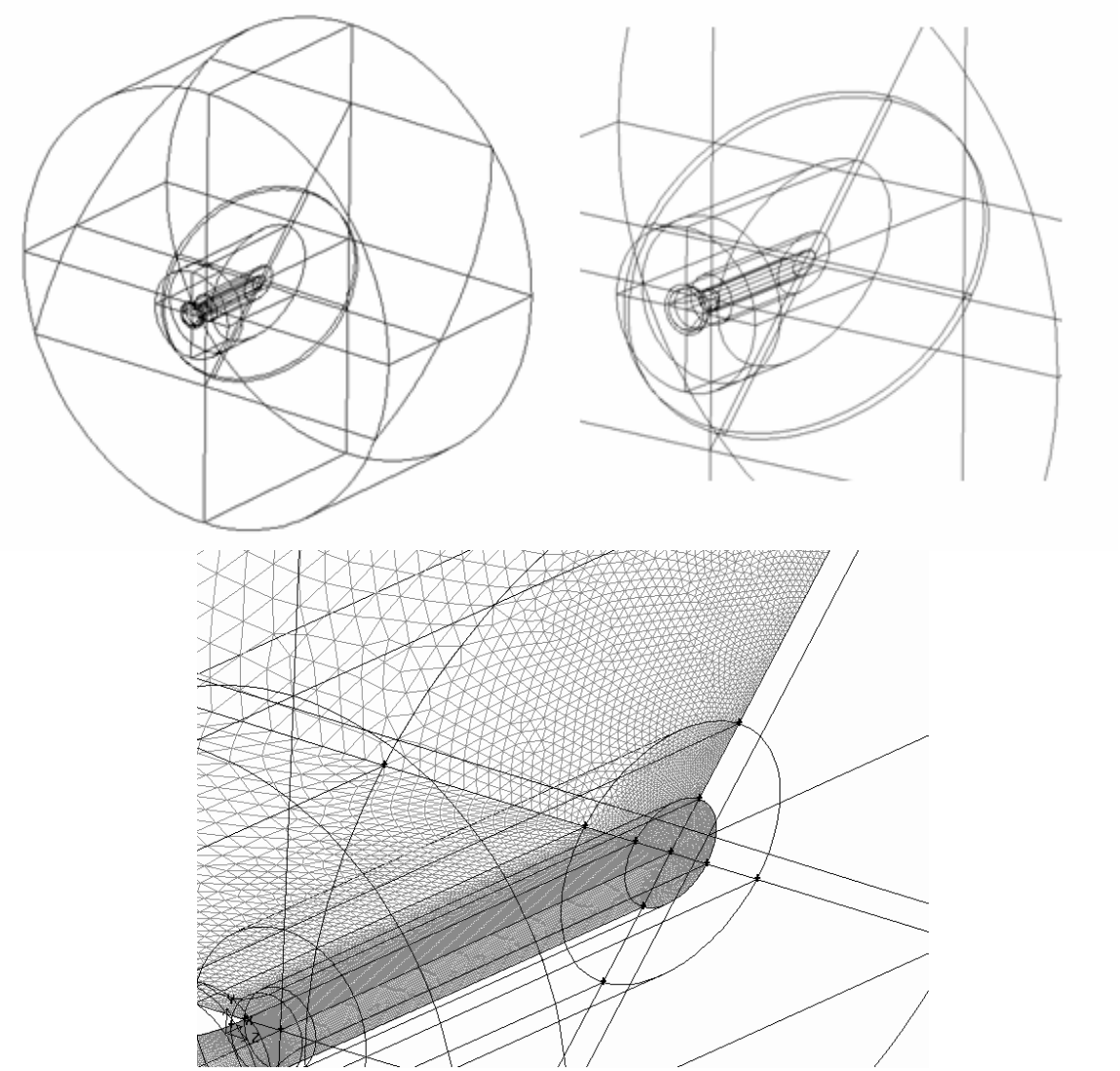

Figure 4.26. The solution space used to model the impingement of a moderately underexpanded jet onto a circular disk at 45º.

An unstructured 3-D grid composed of tetrahedral elements was applied to the domain resulting in an initial resolution of 1,500,000 cells. After obtaining a steady solution, the grid was adapted to obtain greater resolution in the areas of high gradients. The resulting grid resolution was approximately 2,100,000 cells. Contours of velocity magnitude obtained from the computational model are presented in Figure 4.24. As with the previous impingement study, a similar flowfield was observed. Adapting to gradients

of turbulence intensity ensured that the interaction of the high speed jet and the quiescent air were modeled correctly.

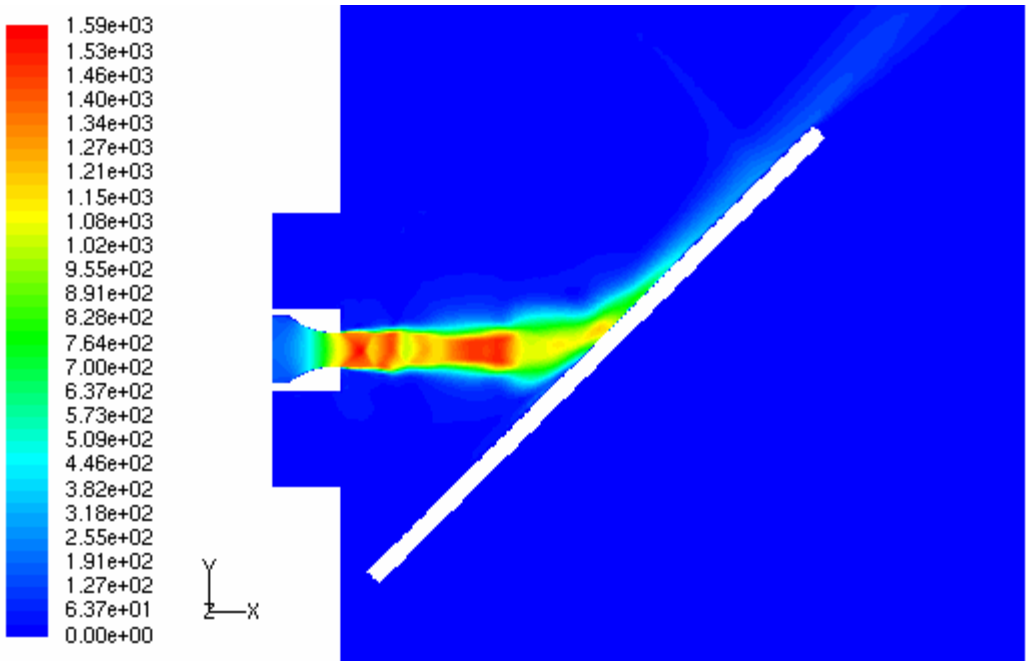

Figure 4.27. Velocity contours obtained for the impingement of a moderately underexpanded onto a 45° disk.

Wall jet velocity profiles were computed at intervals of 30° around the disc and compared to experimental results. A comparison of the numerical and experimental wall velocity profiles for the 12 o'clock position is provided in Figure 4.28. As in the 60° case, very close agreement with the experimental was observed. However, the results also demonstrate that the resolution of the boundary layer could be improved. With further refinement of the computational grid, the results should converge.

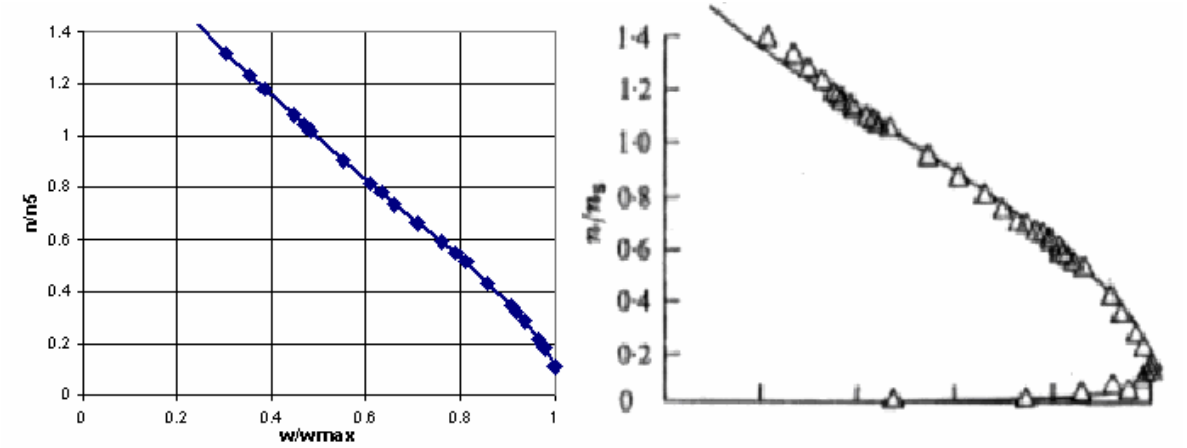

Figure 4.28. Computational (left) and experimental (right) results for a moderately underexpanded jet impinging on a 45º disk.

The dependence of wall jet non-dimensional maximum velocity on azimuthal rake position for the 60° and 45° impingement cases were also compared to experimental results. The results presented in Figure 4.29 provide an estimate of the spreading rate associated with the impingement of the circular jet onto the disk. The normalized error corresponding to the 60° and 45° impingement cases were found to be 2.98% and 1.23% respectively. The strong agreement between computational and experimental data suggests that FLUENT is able to accurately predict the flowfield associated with high speed jet impingement.

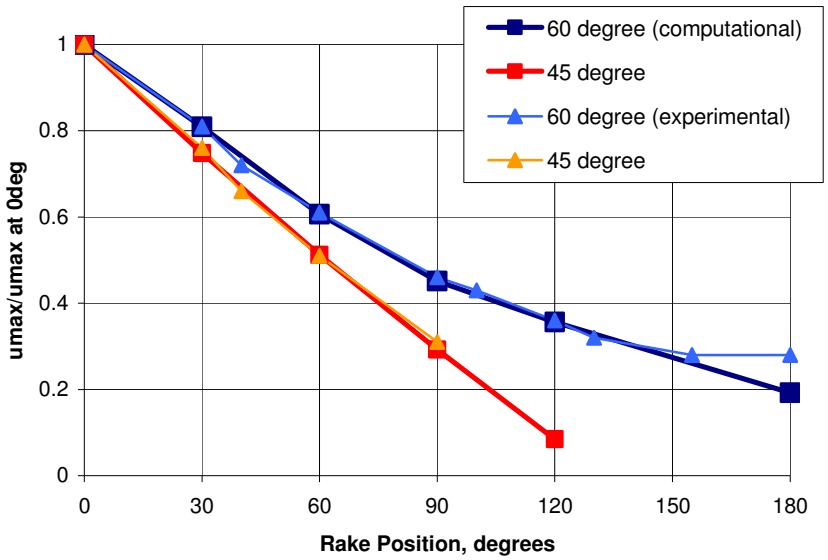

Figure 4.29. Computational and experimental results for the dependence of wall jet non-dimensional maximum velocity on azimuthal rake position.

5 Summary, Conclusions, and Recommendations

5.1 Summary of Free Jet Analysis

Through the analysis of a computational model for a 3-D free jet, the ability of FLUENT to accurately model subsonic and underexpanded jets has been confirmed. By first analyzing axisymmetric cases, the combination of CFD solvers and mesh resolution that provided the greatest accuracy and stability was determined. Full 3-D cases then confirmed that the entire flow field corresponding to the high speed jet could be modeled accurately. The realizable k-ε viscous model along with the 2^{nd} order accurate, segregated, implicit solver provided the greatest agreement with experimental results. In order to ensure a converged solution, grid adaption to gradients of turbulence intensity was applied. Successful validation of the high speed jet was obtained for a Mach 0.57 flow with a pressure ratio of 1.0, a Mach 1.0 flow with a pressure ratio of 1.42, and a Mach 1.0 flow with a pressure ratio of 3.57.

For each of the cases studied in this investigation, it was observed that the velocity profile data near the nozzle exit provided the closest prediction to the experimental data. One contributing factor to this result is due to the decreased resolution at the pressure outlet boundary downstream of the nozzle. The outlet region does not experience the high level of gradients the inlet region does and as a result, requires less resolution to obtain a converged solution. Therefore, less grid adaption was applied to this region. For each of the cases, the velocity profile data taken at a distance of $z/d_n = 1.96$ resulted in the most accurate prediction of the experimental results. Inaccuracies with the prediction of the flowfield are also known to be due to experimental error. As previously mentioned, Donaldson and Snedeker [1] were aware that

unsteadiness and turbulence inherent in these high speed jets can be problematic for measurements taken through pitot and static pressure probes. Further validation of the computational model to more complete experimental data may provide further insight into the true accuracy of the solutions.

5.2 Summary of Jet Impingement Analysis

A computational model to predict the flowfield resulting from the impingement of a moderately underexpanded jet was analyzed. A solution domain was created according to the specifications provided in the study of high speed jet impingement conducted by Donaldson and Snedeker [1]. The solver models and algorithms used in the computational model for the analysis of free jets provided the desired level of stability and accuracy. This included use of the realizable k-ε viscous model along with the 2^{nd} order accurate, segregated, implicit solver. Discretization of the governing equations was completed through 2^{nd} order upwind schemes. After an initial solution was obtained, grid adaption techniques were used to improve the resolution of the computational grid within regions of high gradients.

Experimental results, including wall jet velocity profiles on the surface of the disk, provided the necessary data for validation of the computational model. Converged solutions were obtained for the impingement of a moderately underexpanded jet onto disks rotated 60° and 45° relative to the axis of the jet. Predicted wall jet velocity profiles and velocity distributions on the surface of the disk exhibited strong agreement with the experimental data. However, in the region within the boundary layer of the wall jet profile, more resolution is desired. Development of this computational model

demonstrates the ability of FLUENT to accurately predict the flowfield resulting from the impingement of high speed jets on deflectors. The computational model developed for this investigation can be used to investigate the flowfield associated with passively cooled deflectors.

5.3 Conclusions

A FLUENT model was created for the prediction of flowfields associated with high speed jets and the impingement of underexpanded jets on deflectors. Accuracy of the computational model was assessed through comparison with available experimental data. For each case, there were two main sources of error. These included the extraction of values from graphs provided in published reports and the extrapolation of values in regions where no experimental values were available. Agreement to experimental data was found to range within ±5% for most regions of the flowfield. However, in regions where extrapolation of the data was necessary, large discrepancies were observed with errors ranging from ±10%. Due to the uncertainty in the experimental data, a true assessment of the accuracy can not be provided.

It is the author's assessment that the computational results obtained in this investigation are suitable for guidance in the prediction of free jet flows, impinging flows, and other related devises. The character of the predictions seems to represent believable flow structures in fluid mechanics and fluid dynamics.

5.4 Recommendations for Future Work

The use of CFD for the analysis of high speed jet impingement is an extremely powerful tool. The computational model developed through this investigation provides insight into one of the most highly referenced studies on high speed jets. Use of the parallel version of FLUENT allowed for the entire 3-D flow field to be analyzed. Without having limits on the size of the computational model, the opportunities for applying this method of analysis to other flow fields is seemingly endless.

Although computational results for free and impinging jets compared very well to experimental data, further validation of the computational model should be performed. Specific attention should be focused on the spreading of the free jet as well as the boundary layer of the wall jet after impingement. These are two regions of the flow that displayed the most disagreement. Application of different grid adaption techniques is a suggested method for achieving this validation.

Additionally, a proposed application of this computational model is for the analysis of V/STOL performance. Prediction of hot gas injection as well as other ground effects can be effectively modeled. There has been a considerable amount of experiments related to V/STOL performance, which would provide further validation of the computational model.

6 References

1. Donaldson, C. D. & Snedeker, R. S., "A study of free jet impingement. Part 1. Mean properties of free and impinging jets," *Journal of Fluid Mechanics*, vol. 45, part 2, pp. 281-319, 1971

2. FLUENT^{TM} 6.3.21, FLUENT Inc., 2006

3. Krzywoblocki, M. Z., *Jet Propulsion*, vol. 26, pp. 760-779, 1956

4. Anderson, A. R., & Johns, F. R., *Jet Propulsion*, vol. 25, pp. 13-15, 1955

5. Seddon, J. & Haverty, L., *United Aircraft Corporation Report*, A-1771-24, 1963

6. Owen, P. L. & Thornhill, C. K., *Aero. Res. Council R & M*, 2616, 1952

7. Love, E. S., Grigsby, C. E., Lee, L. P., & Woodling, M. J., "Experimental and theoretical studies of axisymmetric free jets," *NASA TR*, R-6, 1959

8. Hammitt, A. G., "The oscillation and noise of an overpressure sonic jet," *Journal of Aerospace Science*, vol. 28, pp. 673-680

9. Dash, S. M., Pergament, H. S., & Thorpe, R. D., "Computational models for the viscous/inviscid analysis of jet aircraft exhaust plumes," *NASA*, CR-3289, 1980

10. Dash, S. M., Wolf, D. E., & Seiner, J. M., "Analysis of turbulent underexpanded jets, Part 1: Parabolized Navier-Stokes model, SCIPVIS," *AIIAA Journal*, vol. 23, No. 4, 1984

11. Chuech, S. G., Lai, M. C., & Faeth, G. M., "Structure of turbulent sonic underexpanded free jets," *AIAA Journal*, vol. 27, No. 5 1989

12. Woodmansee, M. A. & Dutton, J. C., "Experimental measurements of pressure, temperature, and density in an underexpanded sonic jet flowfield," *30th AIAA Fluid Dynamics Conference*, A99-33660, 1999

13. Henderson, L. F., *Australian Defense Scientific Service,* Mechanical Engineering Note, 238, 1960

14. Lam, C. G. K. & Bremhorst, K. A., "Modified form of the k-ε model for predicting wall turbulence," *Trans. ASME Journal of Fluid Engineering*, Vol. 103, pp. 456-460, 1981

15. Chen, H. C. & Patel, V. C., "Near-wall turbulence models for complex flows including separation," *AIAA Journal*, vol. 26, No. 6, pp. 641-648, 1988

16. Wolfshtein, M., "The velocity and temperature distribution in one-dimensional flow with turbulence augmentation and pressure gradient," *International Journal of Heat & Mass Transfer*, vol. 12, pp. 301-318, 1969

17. Kannenberg, K. C. & Boyd, I. D., "Development of a 3D parallel DSMC code for plume impingement studies," *AIAA Meeting Papers on Disc*, A96-1848, 1996

18. Angioletti, M., Nino, E., & Rucco, G., "CFD turbulent modeling of jet impingement and its validation by particle image velocimetry and mass transfer measurements," *International Journal of Thermal Sciences*, vol 44, pp. 349-356, 2005

19. Brown, G. L. & Roshko, A., "On density effects and large structure in turbulent mixing layers," *Journal of Fluid Mechanics*, vol. 64, part 4, pp. 775-816, 1974

20. Pergament, H. S. & Dash, S. M., "Prediction of nearfield jet entrainment by an interactive mixing/afterburning model," *AIAA 11th Fluid and Plasma Dynamics Conference*, A78-1189, 1978

21. Steffen, C. J., Reddy, D. R., & Zaman, K. B. M. Q., "Numerical modeling of jet entrainment for nozzles fitted with delta tabs," *AIAA Meeting Papers on Disc*, A97-0709, 1997

22. Moore, J. G. & Moore, J., "Realizability in two-equation turbulence models," *30th AIAA Fluid Dynamics Conference*, A99-3779, 1999

23. Rausch, R. D., Batina, J. T., & Yang, H. T. Y., "Spatial adaption procedures on unstructured meshes for accurate unsteady aerodynamic flow computation," *AIAA Structures, Structural Dynamics, and Materials Conference*, A91-1106, 1991

24. Holmes, D. G. & Connell, S. D., "Solution of the 2D Navier-Stokes equations on unstructured adaptive grids," *9th AIAA Computational Fluid Dynamics Conference*, A89-1932-CP, 1989

25. Barth, T. J. & Jespersen, D. C., "The design and application of upwind schemes on unstructured meshes," *27th Aerospace Sciences Meeting*, A89-0366, 1989

Vita

Robert Garcia was born in Alexandria, Louisiana, on July 10, 1982. He grew up on various Air Force bases in the United States and abroad. He graduated High School in 2000, in Fairfax, VA. In the spring of 2005, he earned is Baccalaureate in Mechanical Engineering from Virginia Tech, in Blacksburg, VA. Upon completion of his Master of Science degree in Mechanical Engineering from Virginia Tech in the spring of 2007, he will begin work with the sustainable/green design consulting firm, AKF Engineers, in Philadelphia, PA. CFD will be directly applied to the advancement and application of sustainable buildings.